

We are IntechOpen, the world's leading publisher of Open Access books Built by scientists, for scientists

6,900

Open access books available

185,000

International authors and editors

200M

Downloads

Our authors are among the

154

Countries delivered to

TOP 1%

most cited scientists

12.2%

Contributors from top 500 universities



WEB OF SCIENCE™

Selection of our books indexed in the Book Citation Index
in Web of Science™ Core Collection (BKCI)

Interested in publishing with us?
Contact book.department@intechopen.com

Numbers displayed above are based on latest data collected.
For more information visit www.intechopen.com



Design and Prototyping of a Spherical Parallel Machine Based on 3-CPU Kinematics

Massimo Callegari

*Dipartimento di Meccanica, Università Politecnica delle Marche
Via Brecce Bianche, Ancona,
Italy*

1. Introduction

Parallel kinematics machines, PKMs, are known to be characterised by many advantages like a lightweight construction and a high stiffness but also present some drawbacks, like the limited workspace, the great number of joints of the mechanical structure and the complex kinematics, especially for 6-dof machines. Therefore Callegari *et al.* (2007) proposed to decompose full-mobility operations into elemental sub-tasks, to be performed by separate minor mobility machines, like done already in conventional machining operations. They envisaged the architecture of a mechatronic system where two parallel robots cooperate in order to perform a complex assembly task: the kinematics of both machines is based upon the 3-CPU topology but the joints are differently assembled so as to obtain a translating parallel machines (TPM) with one mechanism and a spherical parallel machine (SPM) with the other.

In one case, joints' axes are set in space so that the mobile platform can freely translate (without rotating) inside its 3D workspace: this is easily obtained by arranging the universal joint of each limb so that the axis of the outer revolute joint is parallel to the base cylindrical joint; such three directions are mutually orthogonal to maximise the workspace and grant optimal manipulability. With a different setting of the joints, three degrees of freedom of pure rotation are obtained at the terminal of the spherical wrist: in this case the axes of the cylindrical joints and those of the outer revolute pairs in the universal joints all intersect at a common point, which is the centre of the spherical motion.

This solution, at the cost of a more sophisticated controller, would lead to the design of simpler machines that could be used also stand-alone for 3-dof tasks and would increase the modularity and reconfigurability of the robotised industrial process. The two robots have been developed till the prototypal stage by means of a virtual prototyping environment and a sketch of the whole system is shown in Fig. 1: while the translating machine has been presented already elsewhere (Callegari & Palpacelli, 2008), the present article describes the design process of the orienting device and the outcoming prototype.

Source: Parallel Manipulators, New Developments, Book edited by: Jee-Hwan Ryu, ISBN 978-3-902613-20-2, pp. 498, April 2008, I-Tech Education and Publishing, Vienna, Austria

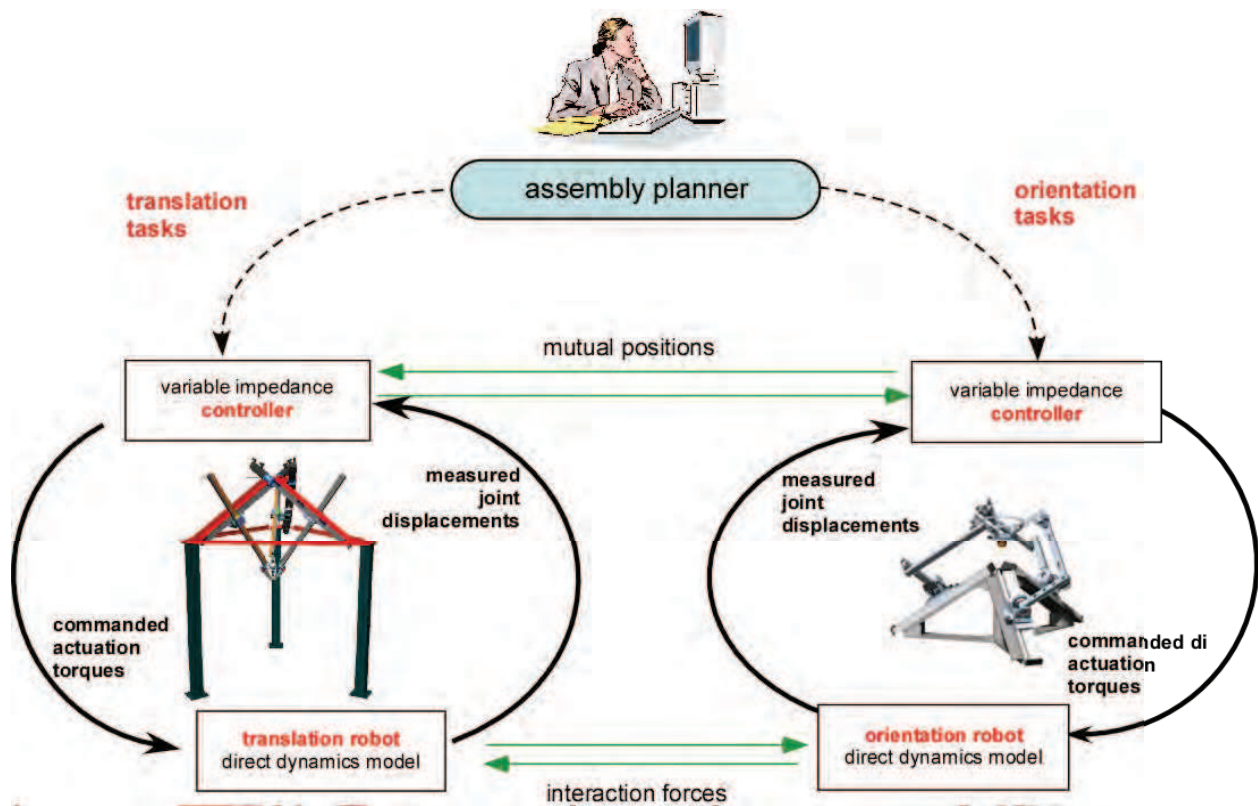


Fig. 1. Architecture of the assembly system based on two cooperating parallel robots

2. Kinematic synthesis

The design of parallel kinematics machines able to perform motions of pure rotation, also called Spherical Parallel Machines, SPM's, is a quite recent research topics: besides the pioneering researches by Asada and Granito (1985), the most important mechanism of this type is the agile eye by Gosselin and Angeles (1989), upon which many prototype machines have been designed since then. Few other studies on the subject are available during the 90's, among which the work of Lee and Chang (1992), Innocenti and Parenti-Castelli (1993) and Alizade *et al.* (1994). In the new millennium, however, a growing interest on spherical parallel wrists produced many interesting results, as new kinematic architectures or powerful design tools. The use of synthesis methods based on or screw theory, for instance, has been exploited by Kong and Gosselin (2004a and 2004b) that provide comprehensive listings of both overconstrained and non-overconstrained SPM's; Hervé and Karouia, on the other hand, use the theory of Lie group of displacements to generate novel architectures, as the four main families in (Karouia & Hervé, 2002) or the 3-RCC, 3-CCR, 3-CRC kinematics specifically treated in (Karouia & Hervé, 2005); Fang and Tsai (2004) use the theory of reciprocal screws to present a systematic methodology for the structural synthesis of a class of 3-DOF rotational parallel manipulators. More interesting architectures, as the 3-URC, the 3-RUU or the 3-RRS, have been studied by Di Gregorio (2001a, 2001b and 2004) and also by other researchers.

Following the approach outlined in (Karouia & Hervé, 2000), Callegari *et al.* (2004) proposed a new wrist architecture, based on the 3-CPU structure; it is noted also that the 3-CRU variant is characterised by a much more complex kinematics but can be useful in view of a

possible prototyping at a mini- or micro- scale, as shown by Callegari *et al.* (2008). The main synthesis steps of the 3-CPU parallel wrist are outlined in the following paragraphs.

First of all, it is noted that only non-overconstrained mechanisms have been searched in order to avoid the strict dimensional and geometric tolerances needed by overconstrained machines during manufacturing and assembly phases. Moreover, the use of passive spherical pairs directly joining the platform to the base has been avoided as well and for economic reasons only modular solutions characterised by three identical legs have been considered. It must be said that these advantages are usually paid with a more complex structure and the possible presence of singular configurations (translation singularities) in which the spherical constraint between platform and base fails.

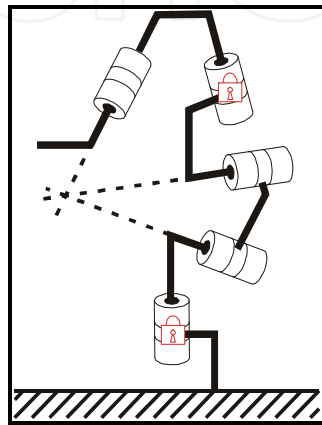


Fig. 2. Limb of connectivity 5 able to generate a spherical motion of the platform

Aiming at this kind of spherical machines, a simple mobility analysis shows that a parallel mechanism able to generate 3-dof motions must be composed by three limbs of connectivity 5. Without losing generality, it is supposed that each single limb consists of 4 links and 5 revolute (R) or prismatic (P) joints that connect the links among them and the limb itself to the fixed frame and to the mobile platform. If each limb's kinematic chain has 3 revolute pairs whose axes intersect at a common point, that is the centre O of the SPM, therefore the moving platform can rotate around the fixed point O: in this way, each limb generates a 5-dimensional manifold that must contain the 3-dimensional group of spherical motions around the point O. If the other two lower pairs are locked, the kinematic chain of the overconstrained Gosselin and Angeles wrist (1989) is obtained, see Fig. 2.

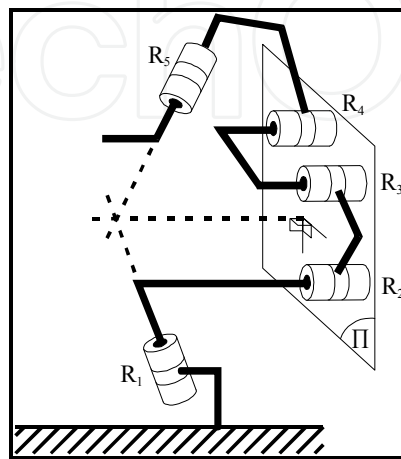


Fig. 3. Limb with subgroup RRR able to generate the subgroup of planar displacements

By analysing the described configuration, it is seen that the spherical motion can be obtained also by using 5 revolute pairs R_1 - R_5 where the axes of the joints R_1 , R_3 and R_5 still intersect at a common point while the axes of pairs R_2 and R_4 are parallel to the direction of R_3 . In such a way, the 3 joints R_2 , R_3 and R_4 will generate the 3-dimensional subgroup of planar displacements $G(\Pi)$, i.e. the set of translations lying in Π and rotations around axes perpendicular to Π . The same subgroup $G(\Pi)$ is generated also in case the axis of revolute joint R_3 is still perpendicular to plane Π but does not cross the rotation centre O , as shown in Fig. 3, therefore also with this limb kinematics a spherical wrist can be obtained.

On the other hand, by following the same line of reasoning, the same subgroup of planar displacements $G(\Pi)$ can be generated by substituting one or two revolute joints among the R_2 , R_3 , R_4 set with prismatic pairs whose axes lie in the plane Π , thus obtaining limbs whose central joints are characterised by one of the sequences PRR, RPR, PPR, PRP, RRP, RPP. Of course, two adjacent joints in limbs kinematics can be merged to yield simpler architectures with fewer links: for instance two revolute joints with orthogonal axes can be superimposed to give a universal (U) joint, while the set of one revolute joint and one prismatic pair with the same axes are equivalent to a cylindrical (C) joint, as shown in Fig. 4.

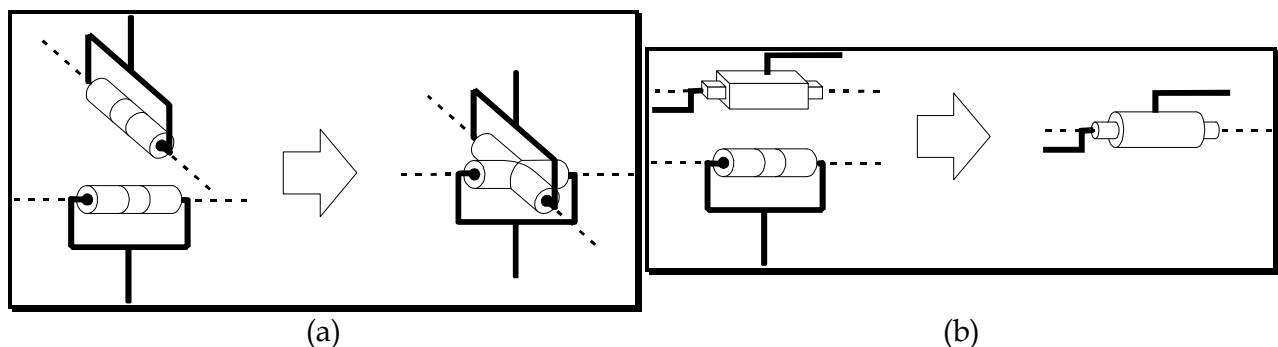


Fig. 4. Merge of two adjacent joints able to yield universal (a) or cylindrical (b) pairs

The kinematic chains described above prevent the i^{th} limb's end from translating in the direction normal to the plane Π_i , $i=1,2,3$; therefore, if three such chains are used for the limbs and the three normals to the planes Π_i are linearly independent, all the possible translations in space are locked and the mobile platform, attached to the three limbs, can only rotate around a fixed point.

In this way, seven alternative design concepts have been considered, which are: 3-URU, 3-CRU, 3-URC, 3-UPU, 3-CPU, 3-UPC, 3-CRC. Figures 5-9 show the mentioned synthesis steps leading to the specific limb topology (a) and sketch a first guess arrangement of the introduced joints (b). In particular, the second picture in each one of these figures, labelled (b), shows the simplest possible setting of the limbs, that all lie within vertical planes: unfortunately in this case the 3 normals to limbs' planes are all parallel to the horizontal plane and therefore result linearly dependent, allowing the platform to translate along the vertical direction, see Fig. 10a. Among all the possible setting of these normal axes in space that grant them to be linearly independent, it has been chosen to tilt the limbs' planes so that they are mutually orthogonal in the initial configuration (or "home" position of the wrist), Fig. 10b, thus greatly simplifying the kinematics relations that will be worked out later on; moreover, even if this arrangement changes during operation of the machine, this configuration is the most far from the singular setting previously outlined, therefore granting a better kinematic manipulability of the wrist. The sketch of the outcoming mechanisms are drawn in Fig. 11-13.

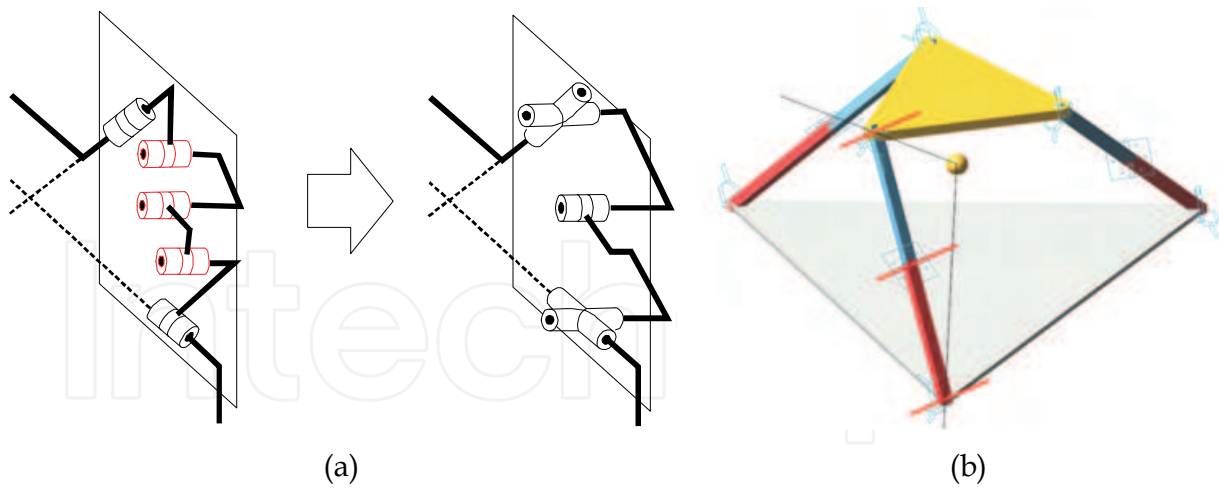


Fig. 5. Synthesis of URU limbs (a) and sketch of the 3-URU mechanism (b)

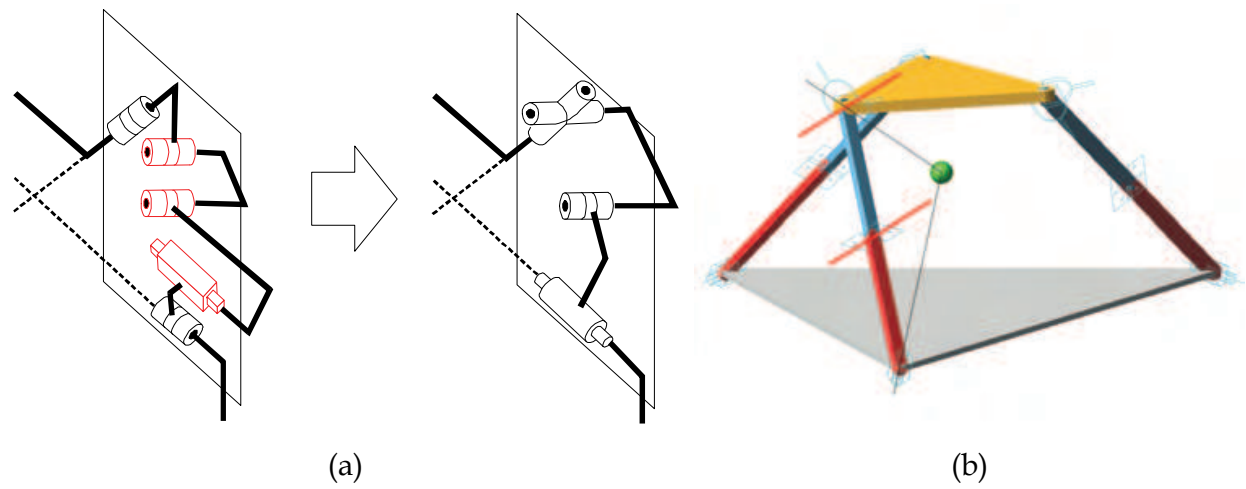


Fig. 6. Synthesis of CRU and URC limbs (a) and sketch of the 3-CRU mechanism (b)

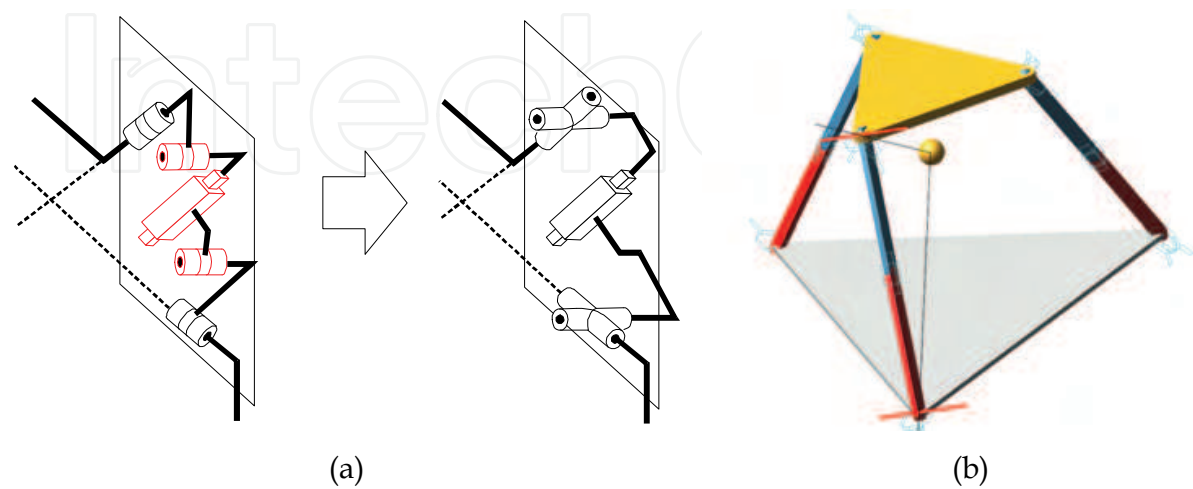


Fig. 7. Synthesis of UPU limbs (a) and sketch of the 3-UPU mechanism (b)

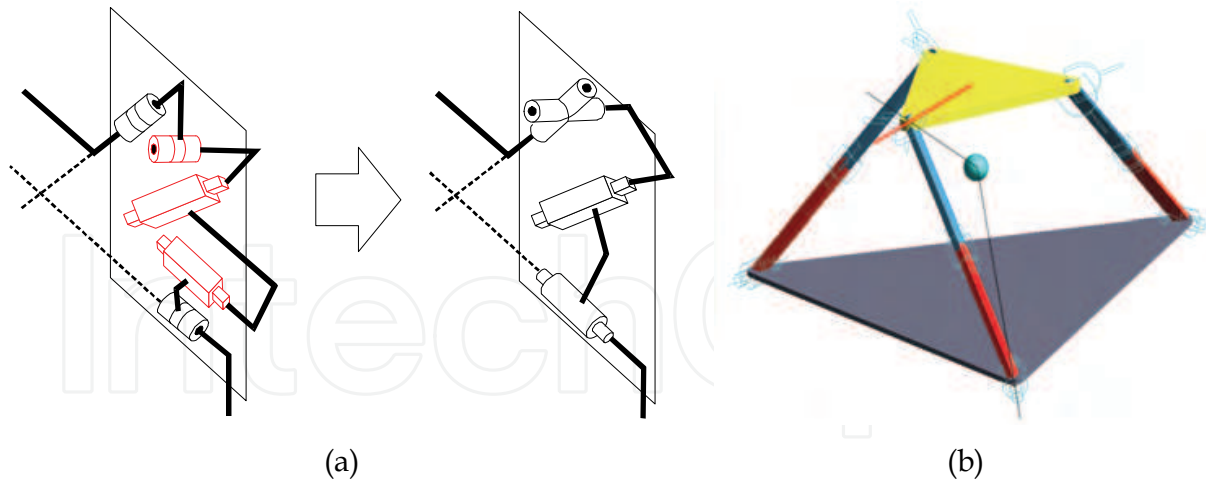


Fig. 8. Synthesis of CPU and UPC limbs (a) and sketch of the 3- CPU mechanism (b)

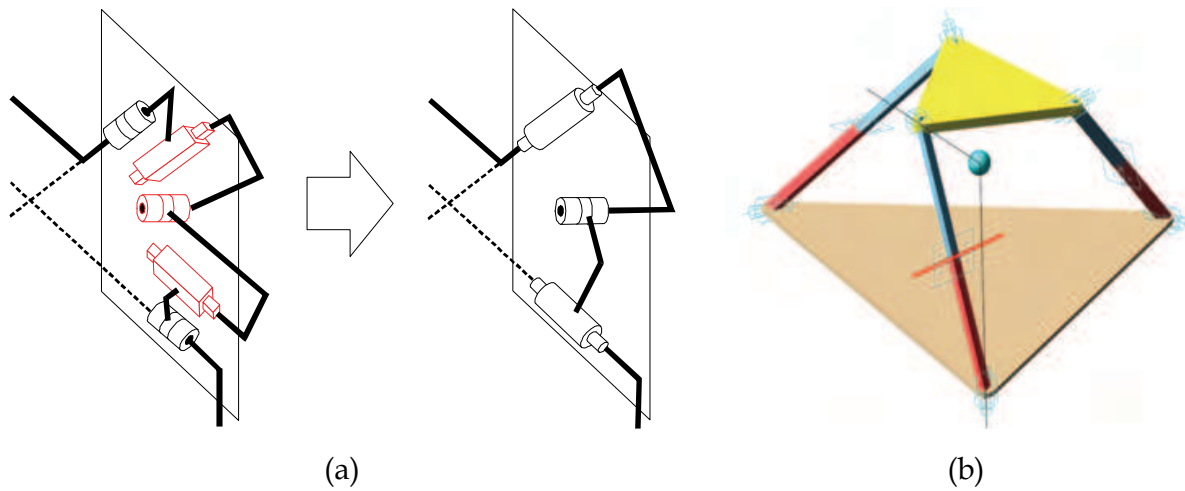


Fig. 9. Synthesis of CRC limbs (a) and sketch of the 3- CRC mechanism (b)

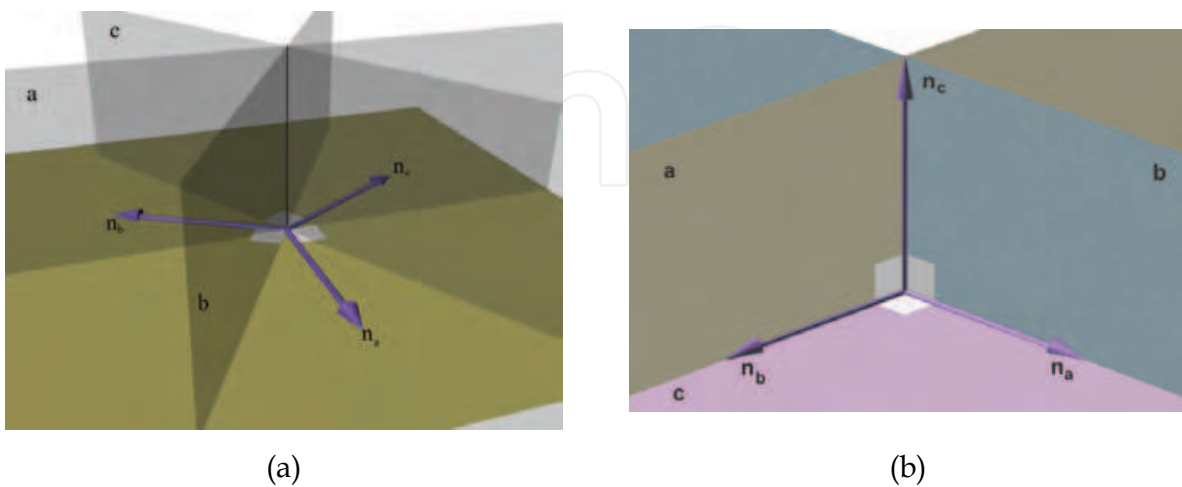


Fig. 10. Setting of the 3 axes normal to limbs' planes: coplanar (a) and orthogonal (b)

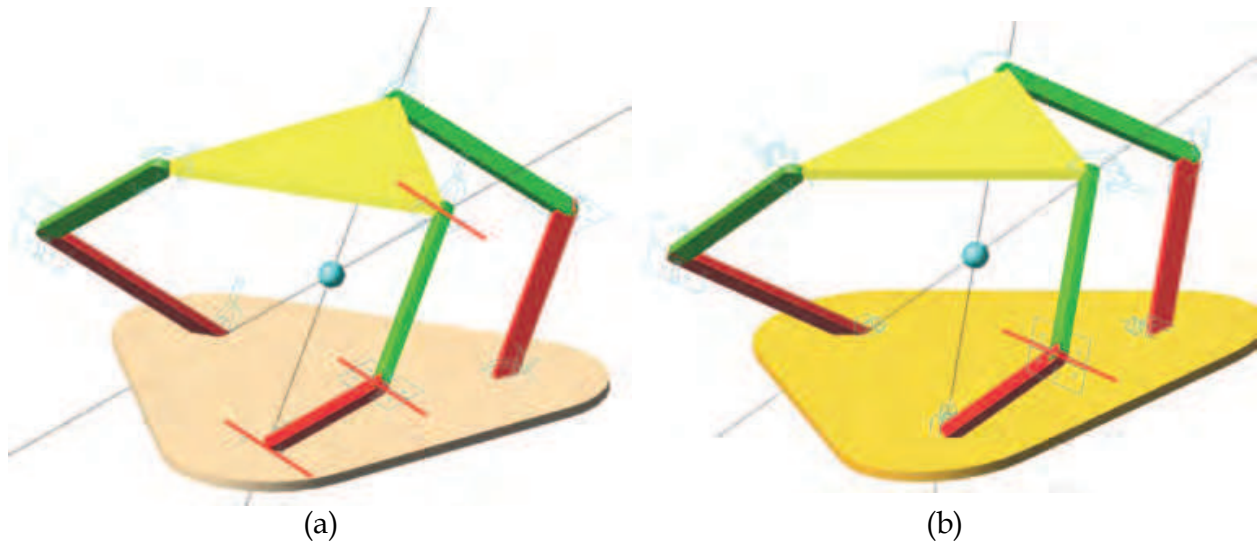


Fig. 11. Concept of a 3-URU (a) and 3-CRU (b) spherical parallel machine (home pose)

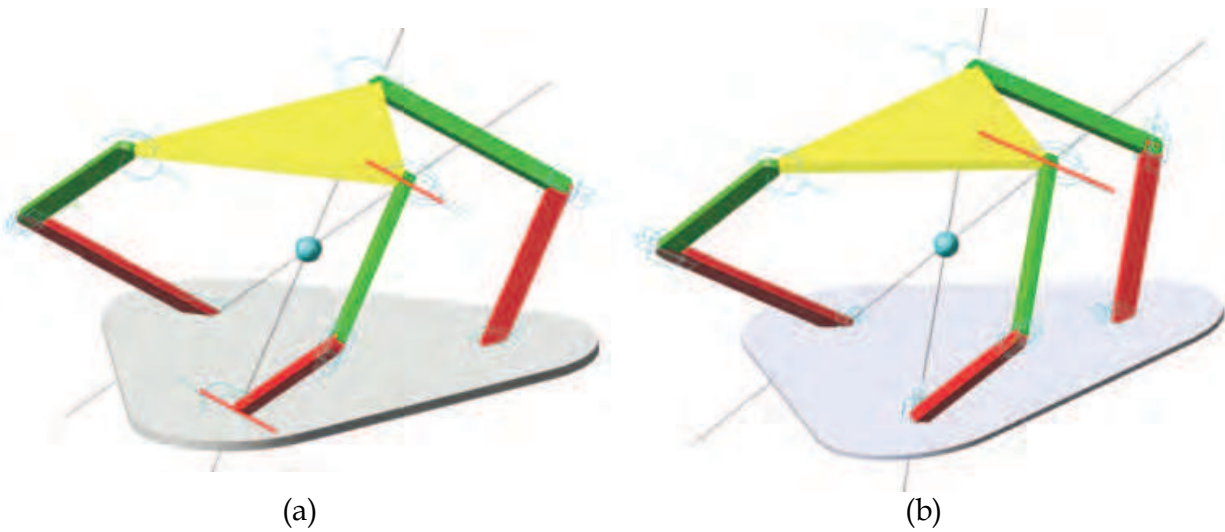


Fig. 12. Concept of a 3-UPU (a) and 3-CPU (b) spherical parallel machine (home pose)

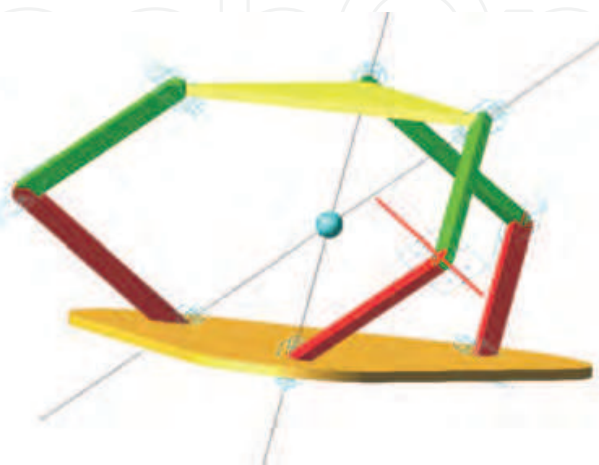


Fig. 13. Concept of a 3-CRC spherical parallel machine (home pose)

The kinematics of such machines has been investigated and in view of the design of a physical prototype the 3-CPU concept has been retained, see Fig. 14: this has been mainly due to the relative simplicity of the kinematics relations that will be worked out in next section, to the compactness of the concept, that allows an easy actuation and finally to the novelty of the kinematics, that has been proposed by Olivieri first (2003) and then studied by Callegari *et al.* (2004). Before studying the kinematics of the 3-CPU SPM it is marginally noted that the same limb's topology, with a different joints arrangement, is able to provide motions of pure translation (Callegari *et al.*, 2005); moreover, the 3-CRU mechanism is extensively studied in (Callegari *et al.*, 2008) in view of the realisation of a SPM for miniaturized assembly tasks.

3. Kinematic analysis

3.1 Description of geometry and frames setting

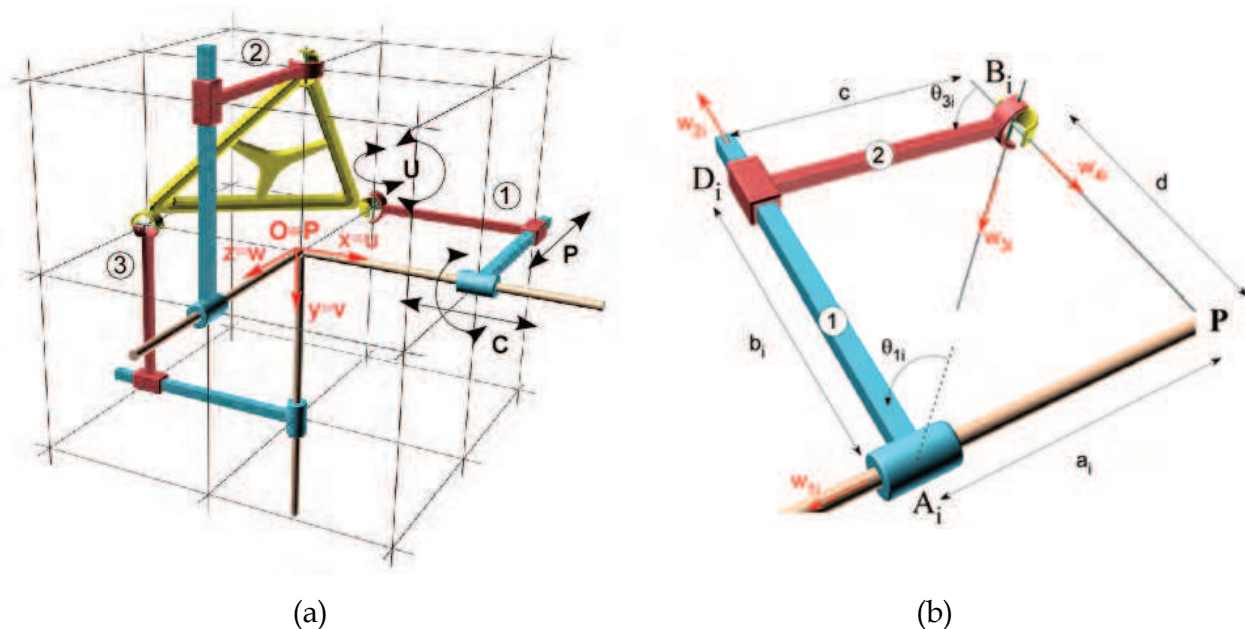


Fig. 14. Placement of reference frames (home pose) (a) and geometry of a single limb (b)

Making reference to Fig. 14, the axes of cylindrical joints A_i , $i=1,2,3$ intersect at point O (centre of the motion) and are aligned to the axes x , y , z respectively of a (*fixed*) Cartesian frame located in O . The first member of each link (1) is perpendicular to A_i and has a variable length b_i due to the presence of the prismatic joint D_i ; the second link (2) of the leg is set parallel the said cylindrical pair. The universal joint B_i is composed by two revolute pairs with orthogonal axes: one is perpendicular to leg's plane while the other intersects at a common point P with the corresponding joints of the other limbs; such directions, for the legs $i=1,2,3$ orderly, are aligned to the axes u , v , w respectively of a (*mobile*) Cartesian frame, located in P and attached to the rotating platform. For a successful functioning of the mechanism, such *manufacturing conditions* must be accompanied by a proper *mounting condition*: assembly should be operated in such a way that the two frames $O(x,y,z)$ and $P(u,v,w)$ come to coincide. Finally, it is assumed an initial configuration such that the linear displacements a_i of the cylindrical joints are equal to the constant length c (that is the same for all the legs): in this case also the linear displacements b_i of the prismatic joints are equal

to the constant length d . It is also evident that, for practical design considerations, SPM's based on the 3-CPU concept are efficiently actuated by driving the linear displacements of the cylindrical pairs coupling the limbs with the frame: therefore in the following kinematic analysis it will be made reference to this case (i.e. joint variables a_i , $i=1,2,3$ will be considered the actuation parameters).

3.2 Analysis of mobility

From the discussion of previous section, it is now evident that in case the recalled manufacturing and assembly conditions are satisfied, the mobile platform is characterised by motions of pure rotation; the mentioned conditions can be geometrically expressed by:

- i. $\hat{\mathbf{w}}_{1i}$ and $\hat{\mathbf{w}}_{4i}$ incident in P ;
- ii. $\hat{\mathbf{w}}_{3i}$ perpendicular to the plane $\langle \hat{\mathbf{w}}_{1i}, \hat{\mathbf{w}}_{4i} \rangle$, i.e. $\hat{\mathbf{w}}_{3i} \cdot \hat{\mathbf{w}}_{4i} = 0$ and $\hat{\mathbf{w}}_{3i} \cdot \hat{\mathbf{w}}_{1i} = 0$;
- iii. $\hat{\mathbf{w}}_{2i}$ lying on the plane $\langle \hat{\mathbf{w}}_{1i}, \hat{\mathbf{w}}_{4i} \rangle$, i.e. $\hat{\mathbf{w}}_{3i} \cdot \hat{\mathbf{w}}_{2i} = 0$; due to condition (ii) must also hold: $\hat{\mathbf{w}}_{3i} = \hat{\mathbf{w}}_{1i} \times \hat{\mathbf{w}}_{2i}$;
- iv. $\hat{\mathbf{w}}_{2i}$ not parallel to $\hat{\mathbf{w}}_{1i}$ and therefore: $\hat{\mathbf{w}}_{1i} \times \hat{\mathbf{w}}_{2i} \neq \hat{\mathbf{0}}$ (for simplicity, the condition $\hat{\mathbf{w}}_{1i} \cdot \hat{\mathbf{w}}_{2i} = 0$ has been posed).

Making reference to Fig. 14b, if the point P is considered belonging to the i^{th} leg, its velocity can be written in three different ways as follows:

$$\dot{\mathbf{P}} = \dot{\mathbf{P}}_{2i} + \dot{\mathbf{P}}_{ri} \quad \text{for } i=1,2,3 \quad (1)$$

where $\dot{\mathbf{P}}_{2i}$ is the velocity of point P if considered fixed to link 2:

$$\dot{\mathbf{P}}_{2i} = \dot{\mathbf{B}}_i + \boldsymbol{\omega}_{2i} \times (P - B_i) = \dot{\mathbf{B}}_i + \boldsymbol{\omega}_{2i} \times d \hat{\mathbf{w}}_{4i} \quad (2)$$

and $\dot{\mathbf{P}}_{ri}$ is the velocity of point P relative to a frame fixed to link 2 and with origin in B_i :

$$\dot{\mathbf{P}}_{ri} = \dot{\theta}_{3i} \hat{\mathbf{w}}_{3i} \times (P - B_i) = \dot{\theta}_{3i} \hat{\mathbf{w}}_{3i} \times d \hat{\mathbf{w}}_{4i} \quad (3)$$

In (2), $\boldsymbol{\omega}_{2i}$ is the angular velocity of link 2:

$$\boldsymbol{\omega}_{2i} = \dot{\theta}_{1i} \hat{\mathbf{w}}_{1i} \quad (4)$$

In the same way, with obvious meaning of the symbols, the vector $\dot{\mathbf{B}}_i$ can be expressed as:

$$\dot{\mathbf{B}}_i = \dot{\mathbf{B}}_{1i} + \dot{\mathbf{B}}_{ri} \quad \text{for } i=1,2,3 \quad (5)$$

where:

$$\dot{\mathbf{B}}_{1i} = \dot{a}_i \hat{\mathbf{w}}_{1i} + \boldsymbol{\omega}_{1i} \times (B_i - A_i) = \dot{a}_i \hat{\mathbf{w}}_{1i} + \dot{\theta}_{1i} \hat{\mathbf{w}}_{1i} \times (a_i \hat{\mathbf{w}}_{1i} - d \hat{\mathbf{w}}_{4i}) = \dot{a}_i \hat{\mathbf{w}}_{1i} - \dot{\theta}_{1i} \hat{\mathbf{w}}_{1i} \times d \hat{\mathbf{w}}_{4i} \quad (6)$$

$$\dot{\mathbf{B}}_{ri} = \dot{b}_i \hat{\mathbf{w}}_{2i} \quad (7)$$

If (2)-(7) are substituted back in (1), it is found:

$$\dot{\mathbf{P}} = \dot{b}_i \hat{\mathbf{w}}_{2i} + \dot{a}_i \hat{\mathbf{w}}_{1i} + \dot{\theta}_{3i} \hat{\mathbf{w}}_{3i} \times d \hat{\mathbf{w}}_{4i} \quad \text{for } i=1,2,3 \quad (8)$$

By dot-multiplying (8) by $\hat{\mathbf{w}}_{3i}$ and by taking into account the conditions (i)-(iv), it is finally obtained:

$$\hat{\mathbf{w}}_{3i} \cdot \dot{\mathbf{P}} = 0 \quad (9)$$

that can be differentiated to yield:

$$\hat{\mathbf{w}}_{3i} \cdot \ddot{\mathbf{P}} + \dot{\hat{\mathbf{w}}}_{3i} \cdot \dot{\mathbf{P}} = 0 \quad (10)$$

Equations (9-10), written for the 3 legs, build up a system of 6 linear algebraic equations in 6 unknowns, the scalar components of $\dot{\mathbf{P}}$ and $\ddot{\mathbf{P}}$. Such a system can be written in matrix form as follows:

$$\mathbf{M} \begin{bmatrix} \dot{\mathbf{P}} \\ \ddot{\mathbf{P}} \end{bmatrix} = \mathbf{0} \quad (11)$$

where the 6x6 matrix \mathbf{M} can be partitioned as:

$$\mathbf{M} = \begin{bmatrix} \mathbf{H} & \mathbf{O} \\ \dot{\mathbf{H}} & \mathbf{H} \end{bmatrix} \quad (12)$$

with:

$$\mathbf{H} = \begin{bmatrix} \hat{\mathbf{w}}_{31}^T \\ \hat{\mathbf{w}}_{32}^T \\ \hat{\mathbf{w}}_{33}^T \end{bmatrix} = \begin{bmatrix} w_{31i} & w_{31j} & w_{31k} \\ w_{32i} & w_{32j} & w_{32k} \\ w_{33i} & w_{33j} & w_{33k} \end{bmatrix} \quad (13)$$

and \mathbf{O} being the 3x3 null matrix.

If the matrix \mathbf{M} is not singular, the system (11) only admits the trivial null solution:

$$\dot{\mathbf{P}} = \ddot{\mathbf{P}} = \mathbf{0} \quad (14-15)$$

which means that the point P does not move in space, i.e. the moving platform only rotates around P . The singular configurations, on the other hand, can be identified by posing:

$$\det(\mathbf{M}) = [\det(\mathbf{H})]^2 = 0 \quad (16)$$

that leads to:

$$\det(\mathbf{H}) = \hat{\mathbf{w}}_{31} \cdot \hat{\mathbf{w}}_{32} \times \hat{\mathbf{w}}_{33} = 0 \quad (17)$$

Equation (17) is satisfied only when the three unit vectors $\hat{\mathbf{w}}_{31}$, $\hat{\mathbf{w}}_{32}$, $\hat{\mathbf{w}}_{33}$ are linearly dependent; therefore the platform incurs in a *translation singularity* if and only if:

- the planes containing the three legs are simultaneously perpendicular to the base plane;
- such planes are coincident with the base plane (configuration not reachable);
- at least two out of the three aforementioned planes admit parallel normal unit vectors.

This justifies the choice previously operated of having the legs laid on mutual orthogonal planes: in fact this configuration is the most far from singularities.

3.3 Orientation kinematics

Orientation kinematics is based on the definition of the relative rotation between fixed frame $O(x,y,z)$ and the mobile frame $P(u,v,w)$, where is always $P \equiv O$, see Fig. 14; to this aim the following set of Cardan angles is used:

$${}^O_P \mathbf{R}(\alpha, \beta, \gamma) = \mathbf{R}_x(\alpha) \cdot \mathbf{R}_y(\beta) \cdot \mathbf{R}_z(\gamma) = \begin{bmatrix} c\beta c\gamma & -c\beta s\gamma & s\beta \\ s\alpha s\beta c\gamma + c\alpha s\gamma & -s\alpha s\beta s\gamma + c\alpha c\gamma & -s\alpha c\beta \\ -c\alpha s\beta c\gamma + s\alpha s\gamma & c\alpha s\beta s\gamma + s\alpha c\gamma & c\alpha c\beta \end{bmatrix} \quad (18)$$

Moreover, a local frame $O_i(x_i, y_i, z_i)$, $i=1,2,3$ is defined for each leg, as shown in Fig. 15: the x_i axis is aligned with cylindrical joint's axis and the y_i axis is chosen parallel to limb's first link, when it is laid in the initial configuration.

One loop-closure equation can be written for each leg as follows:

$$(A_i - P) + (D_i - A_i) + (B_i - D_i) + (P - B_i) = 0 \quad \text{for } i=1,2,3 \quad (19)$$

Equation (19) can be easily expressed in the local frame $O_i(x_i, y_i, z_i)$, $i=1,2,3$:

$$\begin{bmatrix} a_i \\ 0 \\ 0 \end{bmatrix} + \begin{bmatrix} 0 \\ -b_i \cdot c\theta_i \\ -b_i \cdot s\theta_i \end{bmatrix} + \begin{bmatrix} -c \\ 0 \\ 0 \end{bmatrix} + {}^i(P - B_i) = 0 \quad \text{for } i=1,2,3 \quad (20)$$

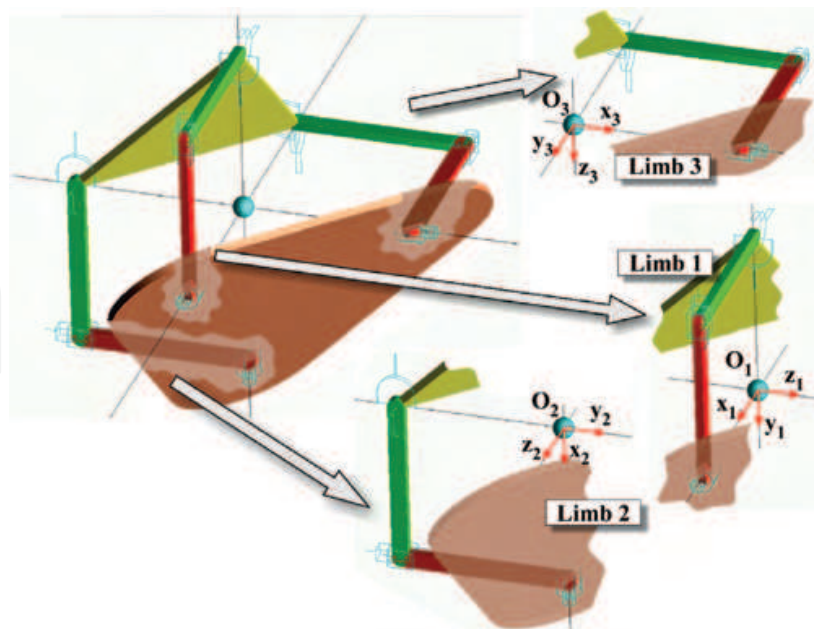


Fig. 15. Setting of local limb frames

The last term in (20) is actually evaluated in the global frame $O(x,y,z)$, then it is transported to limb's frame $O_i(x_i, y_i, z_i)$:

$${}^i(P-B_i) = {}^i\mathbf{R} \cdot {}^P(P-B_i) = {}^i\mathbf{R} \cdot {}^o\mathbf{R} \cdot {}^P(P-B_i) \quad \text{for } i=1,2,3 \quad (21)$$

where the introduced terms assume the following values:

$${}^1\mathbf{R} = \begin{bmatrix} 1 & 0 & 0 \\ 0 & 1 & 0 \\ 0 & 0 & 1 \end{bmatrix} \quad {}^2\mathbf{R} = \begin{bmatrix} 0 & 1 & 0 \\ 0 & 0 & 1 \\ 1 & 0 & 0 \end{bmatrix} \quad {}^3\mathbf{R} = \begin{bmatrix} 0 & 0 & 1 \\ 1 & 0 & 0 \\ 0 & 1 & 0 \end{bmatrix} \quad (22-24)$$

$${}^P(P-B_1) = d \cdot [0 \ 1 \ 0]^T \quad {}^P(P-B_2) = d \cdot [0 \ 0 \ 1]^T \quad {}^P(P-B_3) = d \cdot [1 \ 0 \ 0]^T \quad (25-27)$$

In inverse kinematics the values of α, β, γ Cardan angles (or equivalently the elements r_{ij} of the rotation matrix ${}^o\mathbf{R}$) are known and the joint variables a_i must be found; loop closure equations (21) for $i=1,2,3$ represent three decoupled systems of non linear algebraic equations in the unknowns a_i, θ_{1i} and b_i , that can be solved to find the single solution:

$$\begin{cases} a_1 = c - d \cdot r_{12} \\ \theta_{11} = \text{atan } 2(r_{32}, r_{22}) \\ b_1 = \frac{d \cdot r_{22}}{c \theta_{11}} \end{cases} \quad \begin{cases} a_2 = c - d \cdot r_{23} \\ \theta_{12} = \text{atan } 2(r_{13}, r_{33}) \\ b_2 = \frac{d \cdot r_{33}}{c \theta_{12}} \end{cases} \quad \begin{cases} a_3 = c - d \cdot r_{31} \\ \theta_{13} = \text{atan } 2(r_{21}, r_{11}) \\ b_3 = \frac{d \cdot r_{11}}{c \theta_{13}} \end{cases} \quad (28-30)$$

The direct kinematic problem, on the other hand, assumes the knowledge of joint variables $a_i, i=1,2,3$ and aims at finding the corresponding attitudes of the platform in the space. The analysis is performed by means of simple trigonometric manipulations: by substituting in (28-30) the expression of r_{ij} given in (18), it is obtained:

$$\begin{cases} c\beta s\gamma = \frac{c-a_1}{d} = k_1 \\ s\alpha c\beta = \frac{c-a_2}{d} = k_2 \\ c\alpha s\beta c\gamma - s\alpha s\gamma = \frac{c-a_3}{d} = k_3 \end{cases} \quad (31)$$

where the $k_i, i=1,2,3$ are known values. The 3 equations in (31) can be solved to find up to 4 admissible values for $s\gamma$.

$$\left(2 \frac{k_3 k_2}{k_1} - k_2^2 + 1 + \frac{k_2^2}{k_1^2} \right) s^4 \gamma + (k_3^2 - k_2^2 - k_1^2 - 1) s^2 \gamma + k_1^2 = 0 \quad (32)$$

For each angle γ that solves (32), 2 different values can be found for angles β and α :

$$c\beta = \frac{k_1}{s\gamma} \quad s\alpha = \frac{k_2}{k_1} s\gamma \quad (33-34)$$

therefore system (31) admits up to 16 different solutions: direct kinematics of the mechanism, however, is characterised by a maximum number of 8 different configurations, since angle β can be restricted in the range $[-\pi/2, \pi/2]$ without any loss of information.

3.4 Differential kinematics

By direct differentiation of the first 3 equations in (28-30), the expression of the *analytic Jacobian* \mathbf{J}_A is directly derived:

$$\begin{bmatrix} \dot{a}_1 \\ \dot{a}_2 \\ \dot{a}_3 \end{bmatrix} = d \cdot \begin{bmatrix} 0 & -s\beta s\gamma & c\beta c\gamma \\ c\alpha c\beta & -s\alpha s\beta & 0 \\ -s\alpha s\beta c\gamma - c\alpha s\gamma & c\alpha c\beta c\gamma & -c\alpha s\beta s\gamma - s\alpha c\gamma \end{bmatrix} \cdot \begin{bmatrix} \dot{\alpha} \\ \dot{\beta} \\ \dot{\gamma} \end{bmatrix} = \mathbf{J}_A \begin{bmatrix} \dot{\alpha} \\ \dot{\beta} \\ \dot{\gamma} \end{bmatrix} \quad (35)$$

The *geometric Jacobian* \mathbf{J}_G can be worked out by expressing the relation between the derivatives of Cardan angles and the components of angular velocity $\boldsymbol{\omega}$:

$$\begin{bmatrix} \omega_x \\ \omega_y \\ \omega_z \end{bmatrix} = \begin{bmatrix} 1 & 0 & s\beta \\ 0 & c\alpha & -s\alpha c\beta \\ 0 & s\alpha & c\alpha c\beta \end{bmatrix} \cdot \begin{bmatrix} \dot{\alpha} \\ \dot{\beta} \\ \dot{\gamma} \end{bmatrix} \quad (36)$$

$$\begin{bmatrix} \dot{a}_1 \\ \dot{a}_2 \\ \dot{a}_3 \end{bmatrix} = d \cdot \begin{bmatrix} 0 & -c\alpha s\beta s\gamma - s\alpha c\gamma & c\alpha c\gamma - s\alpha s\beta s\gamma \\ c\alpha c\beta & 0 & -s\beta \\ -s\alpha s\beta c\gamma - c\alpha s\gamma & c\beta c\gamma & 0 \end{bmatrix} \begin{bmatrix} \omega_x \\ \omega_y \\ \omega_z \end{bmatrix} = \mathbf{J}_G \begin{bmatrix} \omega_x \\ \omega_y \\ \omega_z \end{bmatrix} \quad (37)$$

It is noted that the geometric Jacobian \mathbf{J}_G is not a function of geometric parameters, therefore machine's manipulability cannot be optimised by a proper selection of functional dimensions.

3.5 Analysis of singular poses

Limbs' structure does not allow for inverse kinematics singularities, while **direct kinematics singularities** can be found by letting the determinant of \mathbf{J}_G vanish:

$$\det(\mathbf{J}_G) = d^3 [s\beta^2 - (c\alpha c\gamma - s\alpha s\beta s\gamma)^2] \quad (38)$$

The zeros of (38) all lie on closed surfaces in the 3-dimensional space α, β, γ : their intersections with the coordinate planes are straight lines (see also Fig. 16), as given by:

$$\begin{cases} \alpha = 0 \rightarrow \beta \pm \gamma = \pm \pi/2 \\ \beta = 0 \rightarrow \alpha = \pm \pi/2, \gamma = \pm \pi/2 \\ \gamma = 0 \rightarrow \alpha \pm \beta = \pm \pi/2 \end{cases} \quad (39)$$

The analysis of singular configurations has been performed also by means of numerical simulations. Figure 17 shows the value of the determinant of the geometric Jacobian matrix, normalised within the range $[-1, +1]$ after division by the constant d^3 : the black regions are characterised by determinant values in the range $[-0,05, +0,05]$. All the singularity maps are plot against the β and γ angles, α being a parameter of the representation; the configuration

of the mechanism for $\beta=\gamma=0$ is represented aside. Figure 18a plots the singularity surface in the α,β,γ space but it is a hardly readable graph. In Fig. 18b, on other hand, the workspace volumes whose determinant assumes values in the range $[-0,05, +0,05]$ have been taken out of the representation, while the colour map still represents the local determinant value: it is now more appreciable the extent of singularity-free regions inside the workspace, Fig. 18c, where the planning of a motion could be performed: e.g. for the mechanism under design a sphere with a radius of about 50° can be internally inscribed.

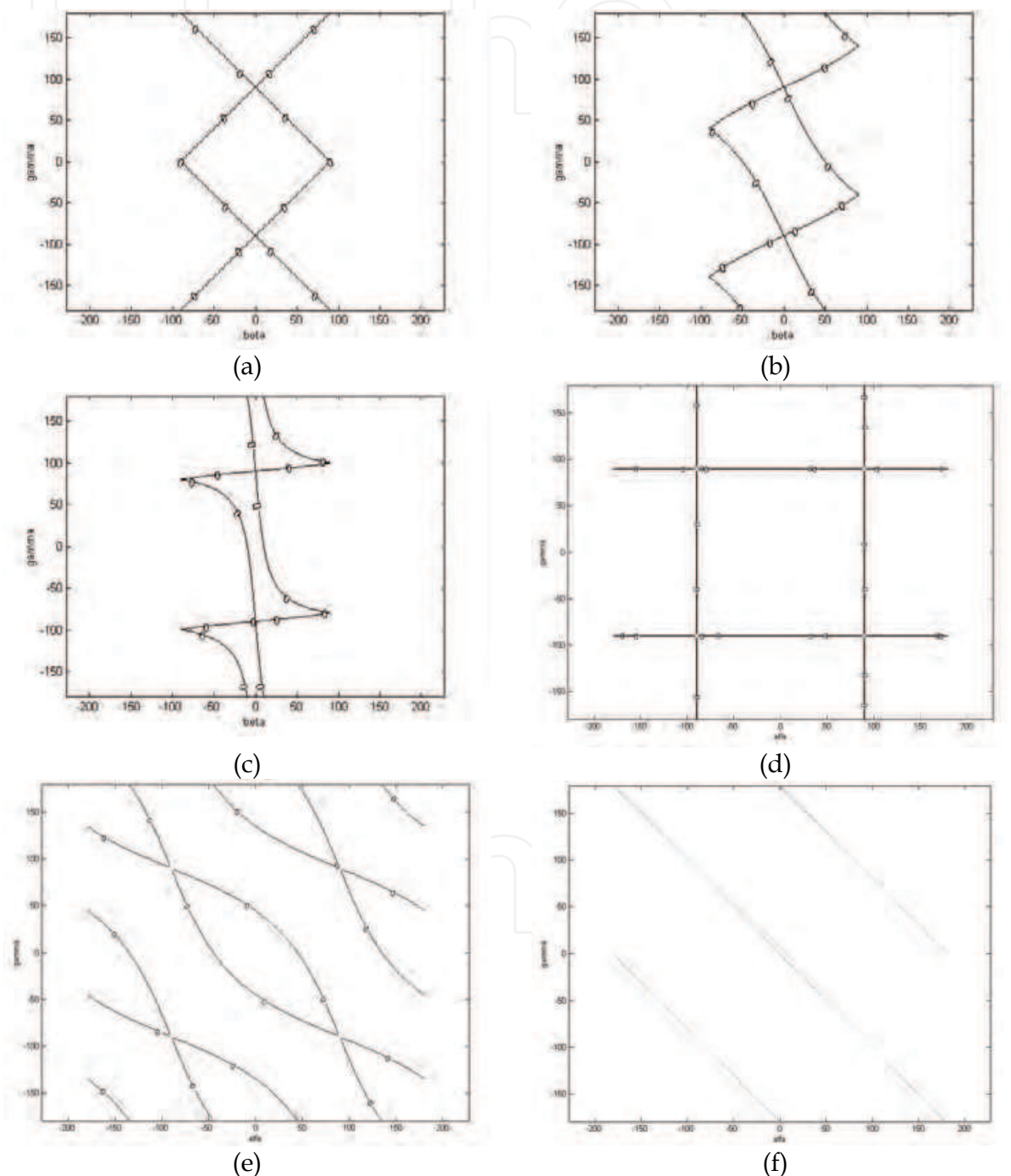


Fig. 16. Projection of direct kinematics singularity surface on several coordinate planes: $\alpha=0^\circ$ (a), $\alpha=40^\circ$ (b), $\alpha=80^\circ$ (c), $\beta=0^\circ$ (d), $\beta=45^\circ$ (e), $\beta=89^\circ$ (f)

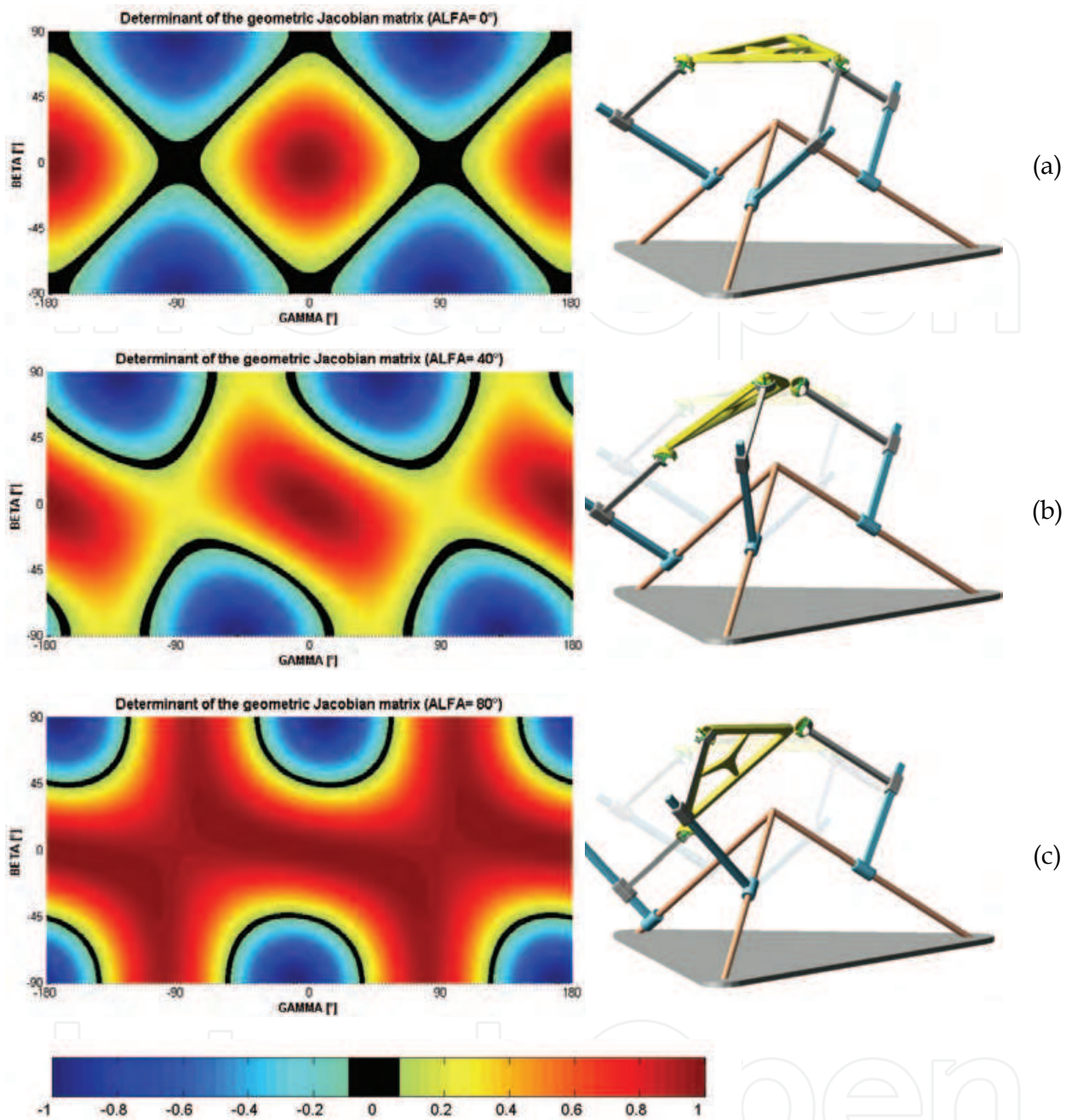


Fig. 17. Determinant of the geometric Jacobian matrix on the planes $\alpha=0^\circ$ (a), $\alpha=40^\circ$ (b), $\alpha=80^\circ$ (c) and representation of manipulator configurations.

The sphere representation of singularity-free regions given in Fig. 18c is suggestive but it is expressed in a space (the α, β, γ Cardan angles) whose geometrical meaning is rather obscure. For many industrial tasks, on the other hand, it may be useful to use the spherical parallel machine for orienting a device or a part within a possibly large 2-dimensional space, identified by the axis of finite rotation, while the need for a further twist around the axis itself may not be urgent or at least only limited rotations may be required. In this case, the geometric Jacobian may be readily represented by a colour map on the surface of a unit sphere. Figure 19, for instance, uses lighter colours to render higher determinant values

while black regions represent almost singular configurations; in this figure the orientation of the platform can be easily read through its elevation and azimuth, with the twist around the central axis is taken as a parameter of the representation: it is noted that in this case, at the expense of reduced twist rotations, greater pointing motions can be accomplished in the other 2 space directions.

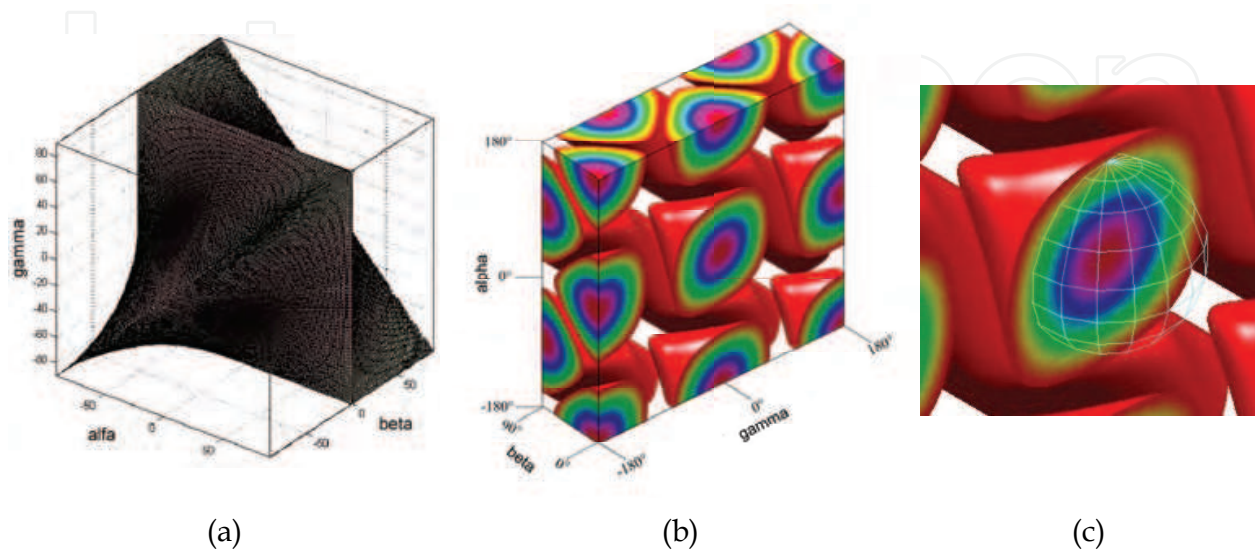


Fig. 18. Singularity surface in the α, β, γ space (a); colour map representing local determinant values (b) and close-up view of a connected singularity-free region.

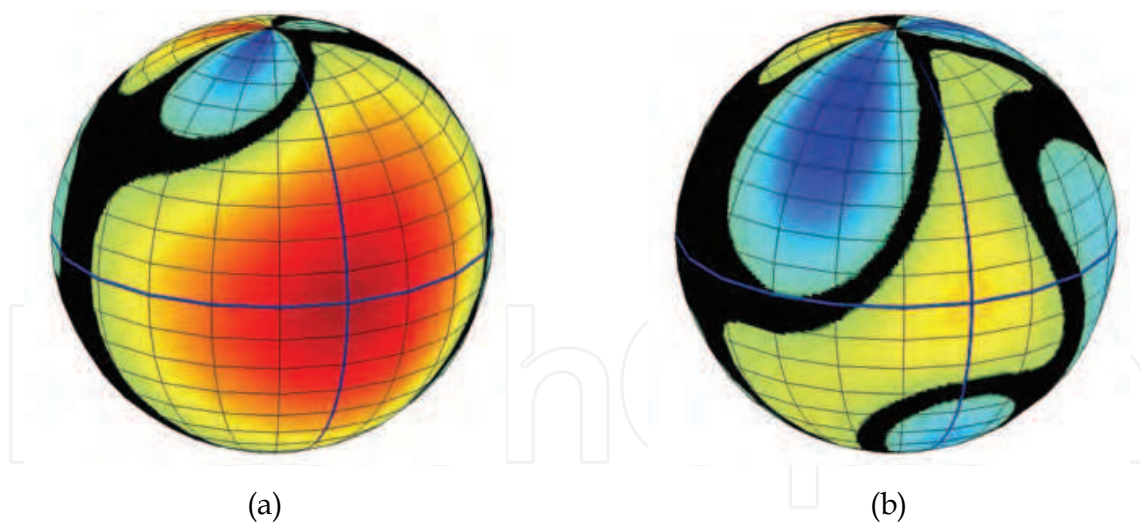


Fig. 20. Singularity-free regions inside workspace for twist angle equal to 20° (a) and 60° (b)

Turning to **translation singularities**, the singular configurations found in (17) can be easily expressed as a function of articular coordinates θ_i :

$$s\theta_1 s\theta_2 s\theta_3 = c\theta_1 c\theta_2 c\theta_3 \quad (40)$$

and taking into consideration inverse kinematics (28-30) it is obtained:

$$r_{32}r_{13}r_{21} = r_{22}r_{33}r_{11} \quad (41)$$

Equation (41) is a useful expression of translation singularities in task space, where the elements of the rotation matrix are used; by using the definition of the rotation matrix in (18) and after some trigonometric manipulation, an alternative expression can be obtained in function of Cardan angles α, β, γ :

$$s\beta^2 - (c\alpha c\gamma - s\alpha s\beta s\gamma)^2 = 0 \quad (42)$$

It is noted that (42) vanishes in the same configurations of (38), therefore translation singularities coincide with direct kinematics singularities, i.e. no additional singular surfaces are present inside workspace.

3.5 Analysis of static loads

The static analysis is useful in the first phases of machine design for the selection of machine's motors and for a first design of the links, with the related connecting bearings. The base relation is provided as usual by the well known duality between kinematics and statics, which allows a straightforward assessment of the actuation efforts τ needed to balance a moment \mathbf{n}_{pl} applied at the mobile platform:

$$\begin{bmatrix} \tau_1 \\ \tau_2 \\ \tau_3 \end{bmatrix} = \mathbf{J}_G^{-T} \begin{bmatrix} n_{plx} \\ n_{ply} \\ n_{plz} \end{bmatrix} \quad (43)$$

It must be noted that the application of a force \mathbf{f}_{pl} at the centre of the spherical motion does not require balancing forces by the actuators but it is entirely born by frame bearings: the internal reactions at the bearings caused by the application of the mentioned external wrench have been evaluated as well and used during structural design.

4. Dynamics

4.1 Inverse dynamics model

In this section an inverse dynamics model of the 3-CPU mechanism is worked out by using the virtual work principle: it is assumed that frictional forces at the joints are negligible, therefore the work produced by the constraint forces at the joints is zero and only active forces (including the gravitational effects) must be accounted in the developments.

In the derivation of the model, the notation is based on Fig. 14b and the second subscript i ($i=1,2,3$) indicates the i^{th} limb while the first subscript j ($j=1,2$) refers to the first or second link respectively. Namely, m_{ji} and I_{ji} are the mass and (central) inertia tensor of the j^{th} member of the i^{th} limb; ω_{ji} is its angular velocity and v_{ji} is the linear velocity of its centre of mass; m_{pl} , I_{pl} , ω_{pl} , v_{pl} are the same quantities referred to the mobile platform.

The total wrench of active and inertial effects acting on the centre of mass of j^{th} member of the i^{th} limb is written as:

$$\mathbf{F}_{ji} \doteq \begin{bmatrix} \mathbf{f}_{ji} \\ \mathbf{n}_{ji} \end{bmatrix} = \begin{bmatrix} m_{ji}\mathbf{g} - m_{ji}\dot{\mathbf{v}}_{ji} \\ -\mathbf{I}_{ji}\dot{\boldsymbol{\omega}}_{ji} - \boldsymbol{\omega}_{ji} \times (\mathbf{I}_{ji}\boldsymbol{\omega}_{ji}) \end{bmatrix} \quad (44)$$

In the same manner, the total wrench acting on the centre of mass of the mobile platform is:

$$\mathbf{F}_{pl} \doteq \begin{bmatrix} \mathbf{f}_{pl} \\ \mathbf{n}_{pl} \end{bmatrix} = \begin{bmatrix} m_{pl}(\mathbf{g} - \dot{\mathbf{v}}_{pl}) + \mathbf{f}_e \\ -\mathbf{I}_{pl}\dot{\boldsymbol{\omega}}_{pl} - \boldsymbol{\omega}_{pl} \times (\mathbf{I}_{pl}\boldsymbol{\omega}_{pl}) + \mathbf{n}_e \end{bmatrix} \quad (45)$$

where \mathbf{f}_e and \mathbf{n}_e are the external force and moment applied to its centre of mass; it is accidentally noted that the centre of mass of the platform does not coincide with the fixed point O. If $\boldsymbol{\tau}$ is the vector of the actuation forces and \mathbf{q} are the corresponding displacements, the principle of virtual work can be written for the present case:

$$(\delta\mathbf{q})^T \cdot \boldsymbol{\tau} + (\delta\mathbf{x}_{pl})^T \cdot \mathbf{F}_{pl} + \sum_{i=1}^3 \left(\sum_{j=1}^2 ((\delta\mathbf{x}_{ji})^T \mathbf{F}_{ji}) \right) = 0 \quad (46)$$

where the vector \mathbf{x}_{ji} gathers the position of the centre of mass of j^{th} member of the i^{th} limb and the orientation of the same link and \mathbf{x}_{pl} expresses the position of the centre of mass of the mobile platform and its orientation. It is noted that all the infinitesimal rotations appearing in (46) must be expressed as functions of the angular velocity of the respective link, e.g. for the platform:

$$\delta\mathbf{x}_{pl} = \begin{bmatrix} v_{plx} & v_{ply} & v_{plz} & \omega_{plx} & \omega_{ply} & \omega_{plz} \end{bmatrix}^T \cdot \delta\mathbf{t} \quad (47)$$

Since all the virtual displacements in (47) must be compatible with the constraints, they are not independent but can rather be expressed as functions of an independent set of Lagrangian coordinates; if the Cardan angles $\boldsymbol{\varphi} = [\alpha, \beta, \gamma]^T$ of the mobile platform are chosen for this purpose, the following relations hold between the introduced virtual displacements:

$$\delta\mathbf{q} = \mathbf{J} \cdot \delta\boldsymbol{\varphi} \quad \delta\mathbf{x}_{ji} = \mathbf{J}_{ji} \cdot \delta\boldsymbol{\varphi} \quad \delta\mathbf{x}_{pl} = \mathbf{J}_{pl} \cdot \delta\boldsymbol{\varphi} \quad (48-50)$$

where \mathbf{J} , \mathbf{J}_{ji} and \mathbf{J}_{pl} are proper Jacobian matrices that can be found through the usual velocity analysis of the mechanism. Equation (46) can be written again as:

$$\delta\boldsymbol{\varphi}^T \cdot \left[\mathbf{J}^T \cdot \boldsymbol{\tau} + \mathbf{J}_{pl}^T \cdot \mathbf{F}_{pl} + \sum_{i=1}^3 \left(\sum_{j=1}^2 \mathbf{J}_{ji}^T \cdot \mathbf{F}_{ji} \right) \right] = 0 \quad (51)$$

Since (51) is valid for any virtual displacement $\delta\boldsymbol{\varphi}$ of the platform, in non-singular configurations it is:

$$\boldsymbol{\tau} = -\mathbf{J}^{-T} \cdot \left(\mathbf{J}_{pl}^T \cdot \mathbf{F}_{pl} + \sum_{i=1}^3 \left(\sum_{j=1}^2 \mathbf{J}_{ji}^T \cdot \mathbf{F}_{ji} \right) \right) \quad (52)$$

Equation (52) completely describes manipulator's dynamics; all the elements in it have been worked out and the resulting model has been proofed by comparison with commercial packages' output, see (Callegari & Marzetti, 2006).

4.2 Dynamic analysis in the task space

The dynamic expression (52) is usefully re-worked in order to explicit the dependency on a proper set of Lagrangian coordinates and its derivatives. In the case of parallel kinematics machines, the dynamic model results quite naturally written in the task space, due to the (usually) difficult expression of DKP; therefore in the present case, after some cumbersome manipulation, it is obtained:

$$\boldsymbol{\tau}_\phi - \mathbf{J}_{pl}^T \mathbf{h} = \mathbf{M}_\phi(\boldsymbol{\phi})\ddot{\boldsymbol{\phi}} + \mathbf{C}_\phi(\boldsymbol{\phi}, \dot{\boldsymbol{\phi}})\dot{\boldsymbol{\phi}} + \mathbf{G}_\phi(\boldsymbol{\phi}) \quad (53)$$

with: $\boldsymbol{\tau}_\phi = \mathbf{J}^T \cdot \boldsymbol{\tau}$, moments acting at the end-effector and corresponding to actual forces $\boldsymbol{\tau}$ at actuated joints; $\mathbf{M}_\phi(\boldsymbol{\phi})$, Cartesian mass matrix of the manipulator; $\mathbf{C}_\phi(\boldsymbol{\phi}, \dot{\boldsymbol{\phi}})$, vector of centrifugal and Coriolis terms; $\mathbf{G}_\phi(\boldsymbol{\phi})$, vector of gravity moments; \mathbf{h} , vector of external forces and moments acting at the centre of mass of the mobile platform.

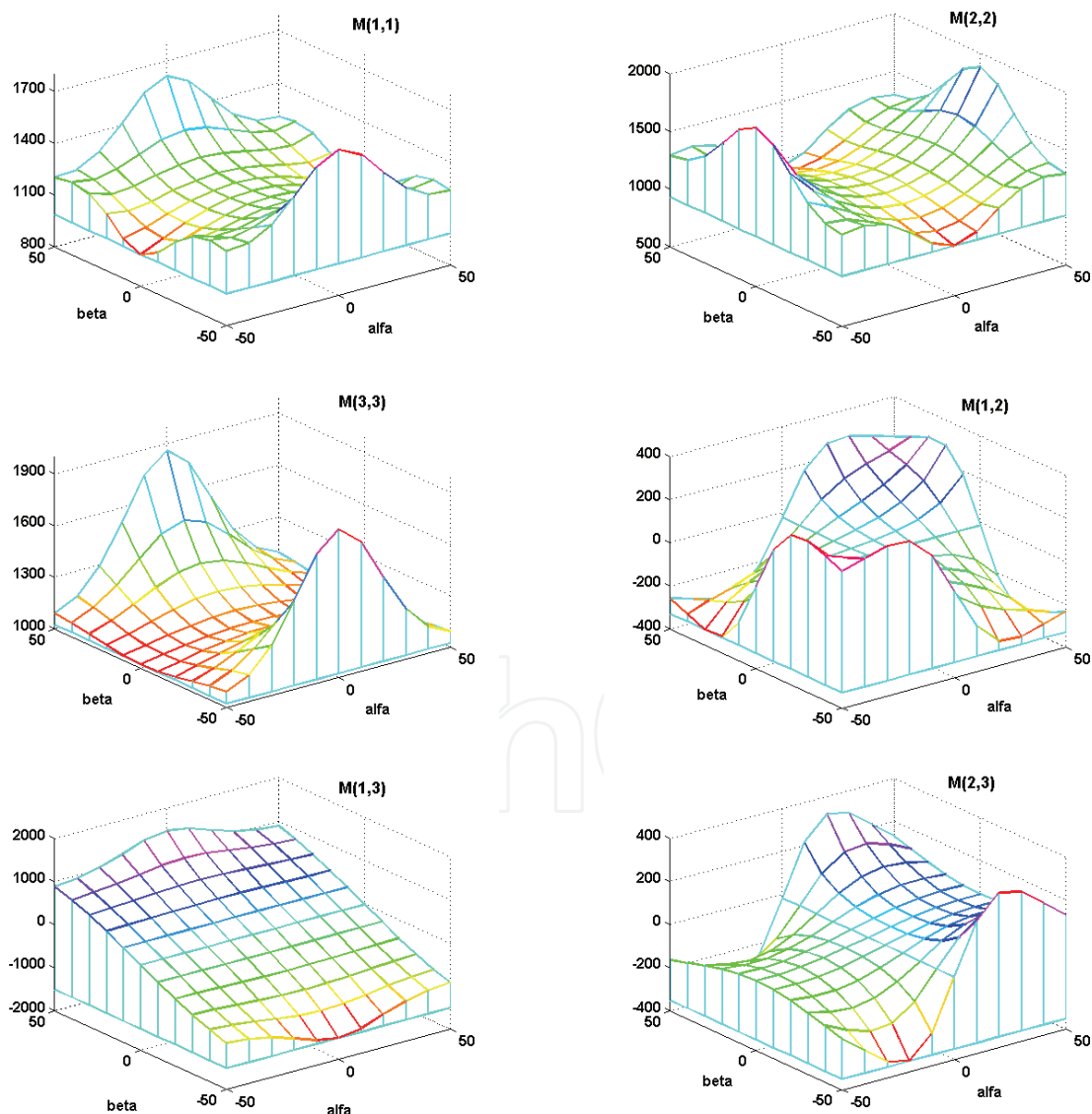


Fig. 21. Values of mass matrix' elements for null roll angle, i.e. $\gamma=0$ (note the different scales of the plots)

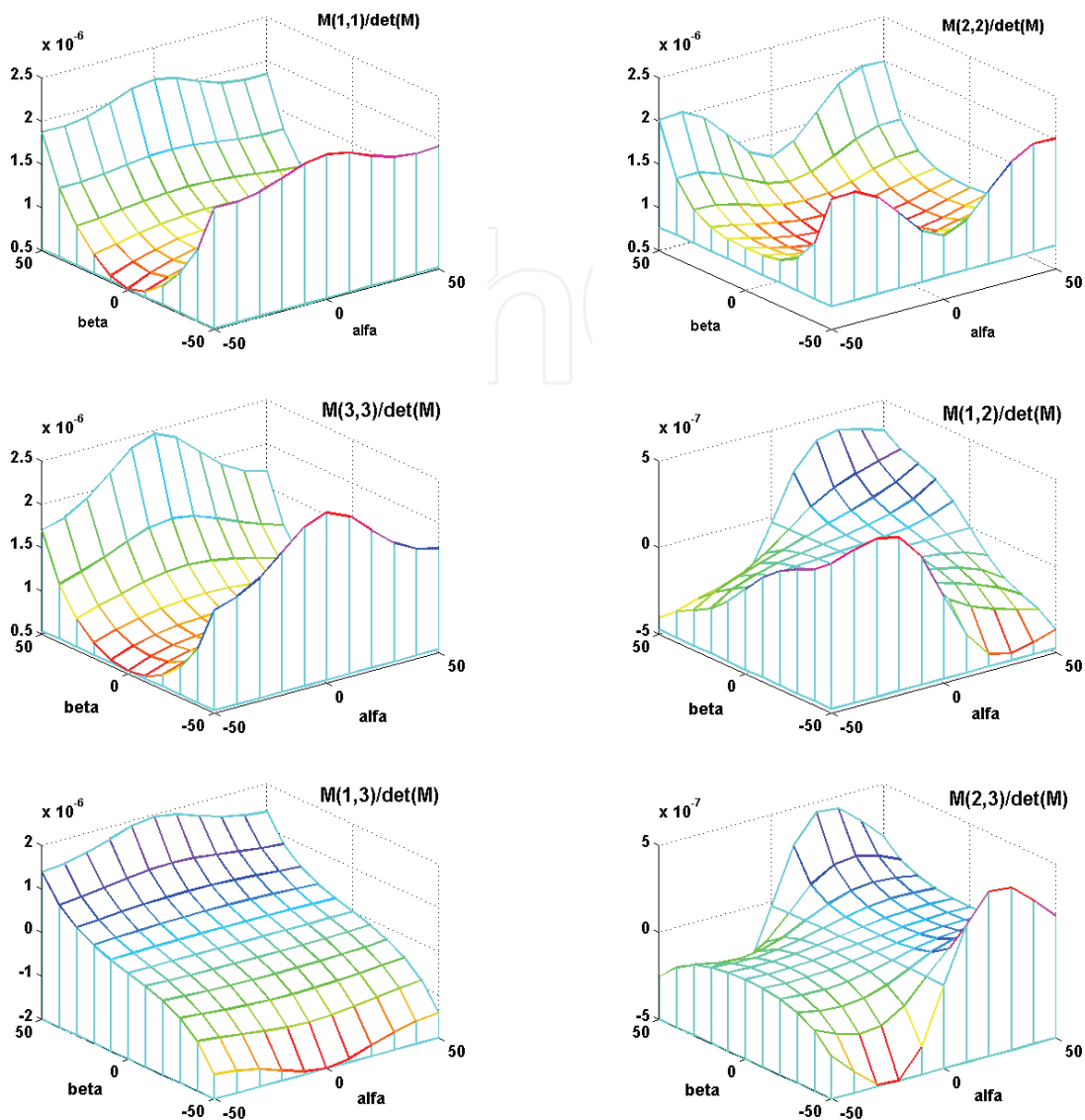


Fig. 22. Plots of mass matrix' elements, normalised by determinant value, for null roll angle, i.e. $\gamma=0$ (note that all the scales of the graphs are multiplied by 10^{-6} but $M(1,2)$ and $M(2,3)$ which are multiplied by 10^{-7})

In view of the realisation of possible control schemes based on the inversion of manipulator's dynamics, it is useful to study the variability of mass matrix throughout the workspace. In fact, a major simplification of the model would be yielded by neglecting the 6 non-diagonal terms of the mass matrix, whether actually allowed by their comparative magnitude; otherwise, all the elements in \mathbf{M}_ϕ and \mathbf{C}_ϕ could be considered constant. First simulation results show that in this case both simplifying assumptions could be taken into consideration, even if the validity of the reduced models weakens when the operating trajectories get closer to singularity surfaces, as expected.

Figure 21, for instance, shows the values of mass matrix' elements in different workspace configurations characterised by null roll angle, i.e. $\gamma=0$: for robot's parameters it has been made reference to the virtual prototype, whose mass properties, presented in the following Tab. 2, are very similar to physical prototype. In Fig. 22 the same plots have been

normalised by dividing the matrix element by the (local) value of matrix determinant, to allow a relative comparison among elements that have very different magnitudes. It can be seen that near the isotropic point ($\alpha=\beta=\gamma=0$) the diagonal elements are dominant and matrix variability is limited, while off-diagonal elements show a stronger influence when getting closer to workspace boundaries; moreover, element $M(3,1)$ is generally an order of magnitude greater than $M(2,1)$ and $M(2,3)$. Such behaviour gets even more evident if one moves away from the plane $\gamma=0$. The plots have been traced for pitch and yaw angles varying between -50° and $+50^\circ$ because the sphere of 50° radius in the Cardan angles space is completely free of singularities, as shown already in Fig. 18.

Other kinds of tests have been performed, aiming at identifying the relative contribute of various dynamic terms: for instance it seems that, even for high dynamics manoeuvres, the contribute of gravity is never negligible, while Coriolis and centrifugal forces account for 10%-16% maximum; on the other hand, the mass and inertia of the mobile platform affect very slightly the overall dynamic behaviour of the machine, possibly allowing for a major simplification of system's model.

4.3 Dynamic manipulability

The dynamic manipulability ellipsoids introduced by Yoshikawa (1985, 2000) are a useful means to study the dynamic properties of a mechanism: they express graphically the capability of a given device to yield accelerations in all the directions stemming from one attitude of its workspace. As a matter of fact, many other measures of manipulability have been proposed by different researchers since that pioneering work but very few applications dealt with orienting devices.

Let us consider all the actuation forces $\boldsymbol{\tau}$ with unit norm:

$$\boldsymbol{\tau}^T \cdot \boldsymbol{\tau} = 1 \quad (54)$$

By manipulating (53) in order to work out $\boldsymbol{\tau}$, it is obtained:

$$\boldsymbol{\tau} = \mathbf{J}^{-T} \mathbf{M}_\varphi (\ddot{\boldsymbol{\phi}} + \ddot{\boldsymbol{\phi}}_{\text{bias}}) \quad (55)$$

having defined:

$$\ddot{\boldsymbol{\phi}}_{\text{bias}} = \mathbf{M}_\varphi^{-1} (\mathbf{C}_\varphi \dot{\boldsymbol{\phi}} + \mathbf{G}_\varphi + \mathbf{J}_{\text{pl}}^T \mathbf{h}) \quad (56)$$

A meaningful formulation of dynamic manipulability must be expressed as a direct function of the angular acceleration $\dot{\boldsymbol{\omega}}$, therefore the mapping between the rate of change of the Cardan angles $\dot{\boldsymbol{\phi}}$ and the angular velocity $\boldsymbol{\omega}$ must be made explicit:

$$\begin{bmatrix} \omega_x \\ \omega_y \\ \omega_z \end{bmatrix} = \begin{bmatrix} 1 & 0 & s\beta \\ 0 & c\alpha & -s\alpha c\beta \\ 0 & s\alpha & s\alpha c\beta \end{bmatrix} \begin{bmatrix} \dot{\alpha} \\ \dot{\beta} \\ \dot{\gamma} \end{bmatrix} \rightarrow \boldsymbol{\omega} = \mathbf{E}(\boldsymbol{\phi}) \dot{\boldsymbol{\phi}} \quad (57)$$

$$\dot{\boldsymbol{\omega}} = \mathbf{E}(\boldsymbol{\phi}) \ddot{\boldsymbol{\phi}} + \dot{\boldsymbol{\omega}}_1(\boldsymbol{\phi}, \dot{\boldsymbol{\phi}}) \quad (58)$$

If $\ddot{\boldsymbol{\phi}}$ is taken out of (58) and substituted in (55) it is then obtained:

$$\boldsymbol{\tau} = \mathbf{J}^{-T} \mathbf{M}_\varphi \mathbf{E}^{-1} (\dot{\boldsymbol{\omega}} + \dot{\boldsymbol{\omega}}_{\text{bias}}) \quad (59)$$

having defined:

$$\dot{\boldsymbol{\omega}}_{\text{bias}} = -\dot{\boldsymbol{\omega}}_1 + \mathbf{E} \mathbf{M}_\varphi^{-1} \mathbf{J}^T \mathbf{M}_\varphi^{-1} (\mathbf{C}_\varphi \dot{\boldsymbol{\phi}} + \mathbf{G}_\varphi + \mathbf{J}_{\text{pl}}^T \mathbf{h}) \quad (60)$$

The constraint expressed by (54) can be finally written in the following quadratic form:

$$\dot{\boldsymbol{\Omega}}^T \cdot \boldsymbol{\Gamma}(\boldsymbol{\varphi}) \cdot \dot{\boldsymbol{\Omega}} = 1 \quad (61)$$

with obvious meaning of the introduced terms:

$$\dot{\boldsymbol{\Omega}} = \dot{\boldsymbol{\omega}} + \dot{\boldsymbol{\omega}}_{\text{bias}} = \dot{\boldsymbol{\omega}} - \dot{\boldsymbol{\omega}}_1 + \mathbf{E} \mathbf{M}_\varphi^{-1} \mathbf{J}^T \mathbf{M}_\varphi^{-1} (\mathbf{C}_\varphi \dot{\boldsymbol{\phi}} + \mathbf{G}_\varphi + \mathbf{J}_{\text{pl}}^T \mathbf{h}) \quad (62)$$

$$\boldsymbol{\Gamma}(\boldsymbol{\varphi}) = \mathbf{E}^{-T} \mathbf{M}_\varphi^T \mathbf{J}^{-1} \mathbf{J}^{-T} \mathbf{M}_\varphi \mathbf{E}^{-1} \quad (63)$$

The inspection of (62-64) shows that gravity merely induces a translation of the dynamic manipulability ellipsoid while in general velocity has a complex, non-negligible effect on manipulability. Making reference to the remarkable case of a fixed platform ($\dot{\boldsymbol{\phi}} = \mathbf{0}$) with no external or gravity action applied ($\mathbf{h} = \mathbf{G}_\varphi = \mathbf{0}$), (61) provides:

$$\dot{\boldsymbol{\omega}}^T \cdot \boldsymbol{\Gamma}(\boldsymbol{\varphi}) \cdot \dot{\boldsymbol{\omega}} = 1 \quad (64)$$

The quadratic form (64) represents an ellipsoid in the Cartesian space of the angular accelerations: its eigenvalues express the square root of the maximum and minimum accelerations that can be developed with unit actuator forces while the eigenvectors represent the associated directions in the orientation space. Figure 23 represents graphically some dynamic manipulability ellipsoids of the robot in the poses sketched aside.

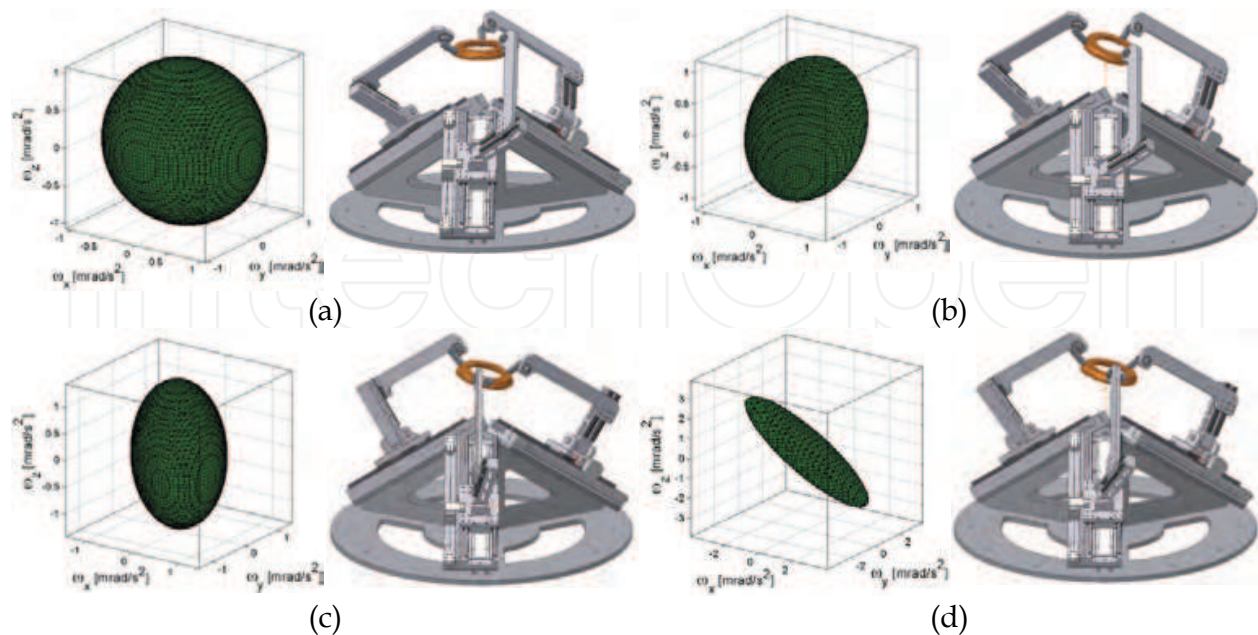


Fig. 23. Dynamic manipulability ellipsoids at different poses (α, β, γ) : $(0^\circ, 0^\circ, 0^\circ)$ (a), $(20^\circ, 20^\circ, -5^\circ)$ (b), $(40^\circ, 40^\circ, 10^\circ)$ (c), $(54^\circ, 53^\circ, 10^\circ)$ (d)

5. Prototype design

The design of a first prototype has been developed, aiming at obtaining high dynamics performances; as reference figures, the following requirements have been posed:

- orientation range (elevation and azimuth): 150°
- maximum angular velocity: $500 \text{ }^\circ/\text{s}$
- maximum angular acceleration: $5\,000 \text{ }^\circ/\text{s}^2$
- spatial resolution: 0.01°
- overall dimensions of the machine: maximum volume of 1 m^3 .

The particular form of the Jacobian matrix (35) does not allow for a mechanical design based on the optimisation of kinematic properties, since \mathbf{J}_G is not function of robot's geometry, therefore heuristic considerations have been made in a first phase, in order to limit wrist's overall dimensions. By looking at Fig. 24 and taking into consideration (31), it is noted that the value of length c does not affect actuators' stroke but only their initial position. The value of length d , instead, is directly proportional to the motors' run needed to attain an assigned configuration in space and by decreasing its value a more compact design is obtained: on the other hand, a lower limit is provided by the need to accommodate the universal joints on the mobile platform and to grant a limit positioning accuracy in the task space. By means of computer simulation, all the geometrical parameters represented in Fig. 24 have been made to change, in order to take into account the above considerations and to assess the resulting geometry; in the end, it has been decided to refine the mechanical design by taking into account the concept of dynamic optimisation, enabled by the availability of the inverse dynamics model.

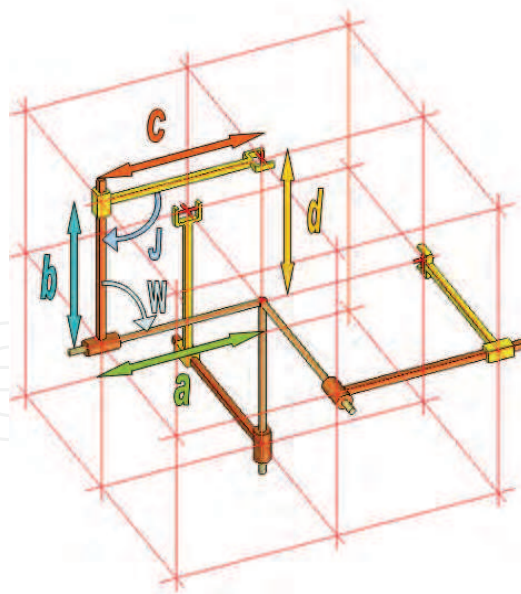


Fig. 24. Main geometrical parameters

Two dynamic figures have been used to drive the design of the machine. The *measure of the dynamic manipulability*, w , defined as:

$$w = \sqrt{\det(\Gamma(\phi))} \quad (65)$$

results proportional to the volume of the manipulation ellipsoid and therefore yields an overall information on the global manipulation capabilities, but fails to capture the closeness to singular configurations or even the anisotropy of local dynamics. On the other hand, the *index of dynamic manipulability*, i , can be defined as:

$$i = \sqrt{\lambda_{\min} / \lambda_{\max}} \quad (66)$$

with λ_{\min} , λ_{\max} minimum and maximum eigenvalues of the matrix $\Gamma(\boldsymbol{\varphi})$: the index (66) is independent from the volume of the ellipsoid and vanishes close to singular configurations.

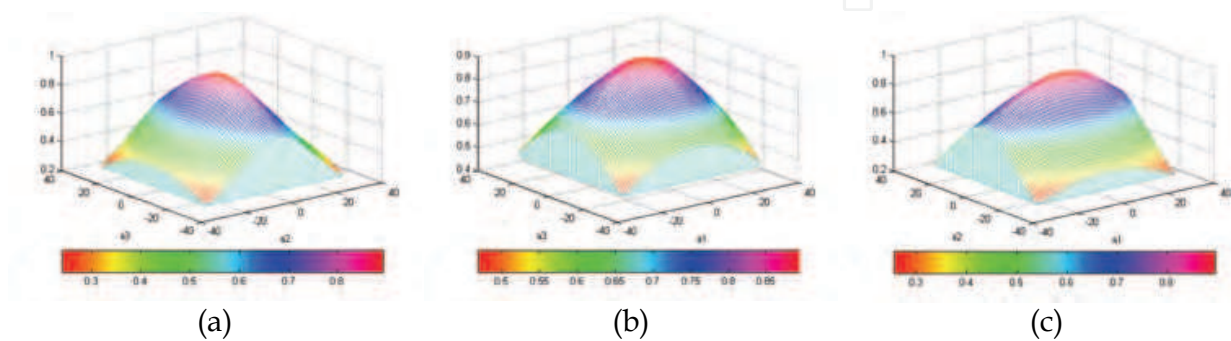


Fig. 25. Plots of the index of dynamic manipulability as a function of actuators strokes on the three coordinate planes $a_1=0$ (a), $a_2=0$ (b), $a_3=0$ (c)

Figure 25 shows sample plots of the index of dynamic manipulability as a function of actuators strokes a_i on the three coordinate planes for the final design. With specific Matlab routines, a dynamic optimisation of the design has been performed, trying to maximise the global dynamic manipulability of the wrist while still guaranteeing a minimum threshold of the local features. For instance, in the configurations shown in Fig. 23a-23d the indexes assume the values: 0.7755, 0.1374, 0.3571, 0.0341 respectively, while it has been obtained a mean value of $i_{ave}=0.502$ over the central $\pm 30^\circ$ span of the workspace. Table 1 summarises the final geometrical values used for the design, with h being the total length of the lower part of the three limbs. It must be said that, as a general rule, in this case the optimisation routines tend to concentrate all the masses in the centre of the spherical motion, that is only too natural.

Figure 26 on the left shows a sketch of the design of final prototype meeting the posed requirements; on the right side, a picture of the machine is presented. The limbs are made of *avional* (an aluminium-copper alloy) in order to join good mechanical properties with a lightweight construction. The mobile platform is made of bronze, therefore allowing the precise machining in a single placement of the 3 journal bearings that have to meet orthogonally in a single point: in this way it has been a high stiffness together with precise geometrical alignments. It must be noted that such revolute joints are idle, since no rotation occurs at all if all the manufacturing and mounting conditions are correctly satisfied. In order to allow the precise mounting of the robot in the initial (home) configuration, the special fixture shown in Fig. 27 has been realised.



Fig. 26. CAD model of spherical wrist (a) and picture of first laboratory prototype (b)

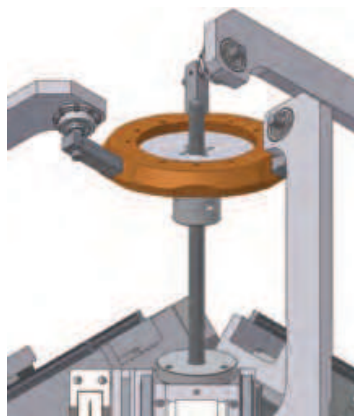


Fig. 27. Sketch of the fixture for axes alignment during machine assembly

The actuation is based on 3 induction linear motors Phase WVS 20.6.3, able to provide a maximum thrust of 184 N at the speed of 6 m/s, with a maximum acceleration of 14.3 g and is controlled by Nation Instrument hardware (Flexmotion/PXI architecture). The first tests of motion are currently under development, while wrist’s controller is under design.

d [mm]	c [mm]	h [mm]	a_{imin} [mm]	a_{imax} [mm]	b_{imin} [mm]	b_{imax} [mm]
210	490	280	319	661	130	210

Tab. 1. Main geometrical data of spherical wrist design

link	m (mass, kg)	I_{11} (x-x moment of inertia, kg m ²)	I_{22} (y-y moment of inertia, kg m ²)	I_{33} (z-z moment of inertia, kg m ²)
upper limb	2.50	0.016	0.016	0.0013
lower limb	7.50	0.070	0.070	0.0014
platform	5.35	0.030	0.030	0.060

Tab. 2. Mass properties of spherical wrist design

6. Conclusions

The article has described an innovative spherical parallel wrist developed at the Polytechnic University of Marche in Ancona, revisiting all the main design steps, from kinematic synthesis up to physical prototyping.

Machine kinematics has been worked out in closed form and all the singularity surfaces have been analysed: it has been pointed out that the mechanism does not possess inverse kinematics singularities, while direct kinematics singularities and translation singularities lie on the same closed surface. The inner space, where motion paths can be safely planned, has been identified and unfortunately it cannot be enlarged by kinematics optimisation because machine's Jacobian does not depend on geometrical parameters.

For this reason, it was decided to drive machine design by dynamic optimisation concepts and an inverse dynamics model has been developed: the study of machine's dynamic manipulability, by means of different algebraic tools, led to the final design of the wrist, that has been also verified with structural analysis packages. The availability of the dynamic model, on the other hand, will be useful for the development of model based control systems, able to exploit the high potentials of direct drive actuation: a first dynamic analysis, moreover, shows that simplified models could be used, since the non-diagonal terms of mass matrix are much smaller than diagonal terms and platform's inertia could be neglected, at least when manipulator is far from singular configurations.

All design steps have been performed in a virtual prototyping environment, that allowed to take into consideration simultaneously the constraints of the mechanics and the problems of the controller, allowing to assess the performances of the closed-loop system. The physical prototyping of the machine, however, allowed to validate the good properties envisaged during the design phase but also to experience the disadvantages of the concept itself: they are mainly due to the scarce accessibility of the centre of the spherical motion, which is common to most parallel wrists, and to the difficult assembly, which requires a precise alignment of joints axes: this problem has been partially overcome by the manufacturing of specific fixtures that are characterised by very high accuracy and are used while assembling the machine.

The machine has been moved so far only through motors drives and a conventional PID position controller is actually being developed: more advanced control systems, able to exploit the high dynamics of the design and the power of direct actuation, will be studied soon.

7. References

- Alizade, R.I.; Tagiyev, N.R. & Duffy, J. (1994) A forward and reverse displacement analysis of an in-parallel spherical manipulator, *Mechanism and Machine Theory*, Vol. 29, No. 1, pp.125-137, ISSN 0094-114X
- Asada, H. & Granito, C. (1985) Kinematic and static characterization of wrist joints and their optimal design, *Proc. IEEE Conf. Robotics and Automation*, pp.244-250, St. Louis, USA, March 25-28.
- Callegari, M. & Marzetti, P. (2006) Inverse Dynamics Model of a Parallel Orienting Device, *Proc. 8th Intl. IFAC Symposium on Robot Control: SYROCO 2006*, Bologna, Italy, Sept. 6-8, 2006.

- Callegari, M. & Palpacelli, M.-C. (2008) Prototype design of a translating parallel robot, *Meccanica* (available on-line at: DOI 10.1007/s11012-008-9116-8), ISSN: 0025-6455.
- Callegari, M.; Gabrielli, A. & Ruggiu, M. (2008) Kineto-Elasto-Static Synthesis of a 3-CRU Spherical Wrist for Miniaturized Assembly Tasks, *Meccanica*, ISSN: 0025-6455.
- Callegari, M.; Gabrielli, A.; Palpacelli, M.-C. & Principi, M. (2007) Design of Advanced Robotic Systems for Assembly Automation, *Intl J. of Mechanics and Control*, Vol. 8, No. 1 (Dec. 2007). pp.3-8, ISSN 1590-8844
- Callegari, M.; Marzetti, P. & Olivieri B. (2004) Kinematics of a Parallel Mechanism for the Generation of Spherical Motions, In: *On Advances in Robot Kinematics*, J. Lenarcic and C. Galletti (Eds), pp.449-458, Kluwer, ISBN 1-4020-2248-4, Dordrecht.
- Callegari, M.; Palpacelli, M.C. & Scarponi, M. (2005) Kinematics of the 3-CPU parallel manipulator assembled for motions of pure translation, *Proc. Intl. Conf. Robotics and Automation*, pp 4031-4036, Barcelona, Spain, April 18-22.
- Di Gregorio, R. (2001a) Kinematics of a new spherical parallel manipulator with three equal legs: the 3-URC wrist, *J. Robotic Systems*, Vol. 18, No. 5 (Apr. 2001), pp.213-219, ISSN 0741-2223
- Di Gregorio, R. (2001b) A new parallel wrist using only revolute pairs: the 3-RUU wrist, *Robotica*, Vol.19, No.3 (Apr. 2001), pp. 305-309, ISSN 0263-5747
- Di Gregorio, R. (2004) The 3-RRS Wrist: A New, Simple and Non-Overconstrained Spherical Parallel Manipulator, *J. of Mechanical Design*, Vol. 126, No. 5, (Sept. 2004) pp.850-855, ISSN 1050-0472.
- Fang, Y. & Tsai, L.-W. (2004) Structure synthesis of a class of 3-DOF rotational parallel manipulators, *IEEE Trans. on Robotics and Automation*, Vol.20, No.1, (Feb. 2004) pp.117-121, ISSN 0882-4967
- Gosselin, C. & Angeles, J. (1989) The optimum kinematic design of a spherical three-degree-of-freedom parallel manipulator, *J. Mechanisms, Transmissions and Automation in Design*, Vol. 111, No 2. pp.202-207, ISSN 0738-0666
- Innocenti, C. & Parenti-Castelli, V. (1993) Echelon form solution of direct kinematics for the general fully-parallel spherical wrist, *Mechanism and Machine Theory*, Vol. 28, No. 4, pp.553-561, ISSN 0094-114X
- Karouia, M. & Hervé, J.M. (2000) A three-dof tripod for generating spherical rotation, In: *Advances in Robot Kinematics*, J.L. Lenarcic & M.M. Stanisic (Eds.), pp.395-402, Kluwer, ISBN 0-7923-6426-0, Dordrecht.
- Karouia, M. & Hervé, J.M. (2002) A Family of Novel Orientational 3-DOF Parallel Robots, *Proc. 14th RoManSy*, pp. 359-368, Udine, Italy, July 1-4.
- Karouia, M. & Hervé, J.M.. (2006) Non-overconstrained 3-dof spherical parallel manipulators of type: 3-RCC, 3-CCR, 3-CRC, *Robotica*, Vol. 24, No. 1, January 2006, pp.85-94, ISSN 0263-5747
- Kong, X. & Gosselin, C.M. (2004) Type synthesis of 3-DOF spherical parallel manipulators based on screw theory, *J. of Mechanical Design*, Vol.126, No.1, (Jan. 2004), pp.101-108, ISSN 1050-0472
- Kong, X. & Gosselin, C.M. (2004) Type synthesis of three-degree-of-freedom spherical parallel manipulators, *Intl J. of Robotics Research*, Vol.23, No.3, (March 2004) pp.237-245, ISSN 0278-3649

- Lee, J.J. & Chang, S.-L. (1992) On the kinematics of the UPS wrist for real time control, *Proc. 22nd ASME Biennial Mechanisms Conference: Robotics, Spatial Mechanisms and Mechanical Systems*, pp.305-312, Scottsdale, USA, Sept. 13-16.
- Olivieri, B. (2003) *Study of a novel parallel kinematics spherical robot for cooperative applications*, Tesi di laurea (in Italian), Università Politecnica delle Marche, Ancona, Italy.
- Yoshikawa, T. (1985). Dynamic Manipulability of Robot Manipulators. *J. Robotic Systems*, Vol. 2, pp.113-124, ISSN 0741-2223.
- Yoshikawa, T. (2000). Erratum to "Dynamic Manipulability of Robot Manipulators". *J. Robotic Systems*, Vol. 17, No. 8, (Aug. 2000), pp.449, ISSN 0741-2223.

IntechOpen



Parallel Manipulators, New Developments

Edited by Jee-Hwan Ryu

ISBN 978-3-902613-20-2

Hard cover, 498 pages

Publisher I-Tech Education and Publishing

Published online 01, April, 2008

Published in print edition April, 2008

Parallel manipulators are characterized as having closed-loop kinematic chains. Compared to serial manipulators, which have open-ended structure, parallel manipulators have many advantages in terms of accuracy, rigidity and ability to manipulate heavy loads. Therefore, they have been getting many attentions in astronomy to flight simulators and especially in machine-tool industries. The aim of this book is to provide an overview of the state-of-art, to present new ideas, original results and practical experiences in parallel manipulators. This book mainly introduces advanced kinematic and dynamic analysis methods and cutting edge control technologies for parallel manipulators. Even though this book only contains several samples of research activities on parallel manipulators, I believe this book can give an idea to the reader about what has been done in the field recently, and what kind of open problems are in this area.

How to reference

In order to correctly reference this scholarly work, feel free to copy and paste the following:

Massimo Callegari (2008). Design and Prototyping of a Spherical Parallel Machine Based on 3-CPU Kinematics, Parallel Manipulators, New Developments, Jee-Hwan Ryu (Ed.), ISBN: 978-3-902613-20-2, InTech, Available from:

http://www.intechopen.com/books/parallel_manipulators_new_developments/design_and_prototyping_of_a_spherical_parallel_machine_based_on_3-cpu_kinematics

INTECH
open science | open minds

InTech Europe

University Campus STeP Ri
Slavka Krautzeka 83/A
51000 Rijeka, Croatia
Phone: +385 (51) 770 447
Fax: +385 (51) 686 166
www.intechopen.com

InTech China

Unit 405, Office Block, Hotel Equatorial Shanghai
No.65, Yan An Road (West), Shanghai, 200040, China
中国上海市延安西路65号上海国际贵都大饭店办公楼405单元
Phone: +86-21-62489820
Fax: +86-21-62489821

© 2008 The Author(s). Licensee IntechOpen. This chapter is distributed under the terms of the [Creative Commons Attribution-NonCommercial-ShareAlike-3.0 License](#), which permits use, distribution and reproduction for non-commercial purposes, provided the original is properly cited and derivative works building on this content are distributed under the same license.

IntechOpen

IntechOpen